Spatio-temporal monitoring by ground-based and air- and space-borne lidars of a moderate Saharan dust event affecting southern Europe in June 2013 in the framework of the ADRIMED/ChArMEx campaign

Ruben Barragan, Michaël Sicard, Julien Totems, Jean-François Léon, François Dulac, Marc Mallet, Jacques Pelon, Lucas Alados-Arboledas, Aldo Amodeo, Antonella Boselli, et al.

Spatio-temporal monitoring by ground-based and air- and space-borne lidars of a moderate Saharan dust event affecting southern Europe in June 2013 in the framework of the ADRIMED/ChArMEx campaign

R. BARRAGAN[1,2], M. SICARD[1,2], J. TOTEMS[3], J.-F. LÉON[5], F. DULAC[3], M. MALLET[4], J. PELON[6], L. ALADOS-ARBOLEDAS[7,8], A. AMODEO[9], P. AUGUSTIN[10], A. BOSELLI[9,12], J. A. BRAVO-ARANDA[7,8], P. BURLIZZI[13], P. CHAZETTE[3], A. COMERÓN[1], G. D'AMICO[9], P. DUBUISSON[10], M. J. GRANADOS-MUÑOZ[7,8], G. LETO[14], J. L. GUERRERO-RASCADO[7,8], F. MADONNA[9], L. MONA[9], C. MUÑOZ-PORCAR[1], G. PAPPALARDO[9], M. R. PERRONE[13], V. PONT[5], F. ROCADENBOSCH[1,2], A. RODRIGUEZ-GOMEZ[1], S. SCOLLO[15], N. SPINELLI[10,16], G. TITOS[7,8], X. WANG[10,17], R. ZANMAR SANCHEZ[14]

1. Remote Sensing Laboratory, Universitat Politècnica de Catalunya, Barcelona, Spain
2. Ciències i Tecnologies de l'Espai - Centre de Recerca de l'Aeronàutica i de l'Espai / Institut d'Estudis Espacials de Catalunya (CTE-CRAE / IEEC), Universitat Politècnica de Catalunya, Barcelona, Spain
3. Laboratoire des Sciences du Climat et de l'Environnement (LSCE), CEA-CNRS-UVSQ, Univ. Paris-Saclay Gif-sur-Yvette, France
4. CNRM UMR 3589, Météo-France/CNRS, Toulouse, France
5. Laboratoire d'Aérologie, Université de Toulouse / CNRS, Toulouse, France
6. Laboratoire Atmosphères, Milieux, Observations Spatiales (LATMOS), Université Pierre et Marie Curie, Paris, France
7. Dpt. Applied Physics, Faculty of Sciences, University of Granada, Fuentenueva s/n, 18071, Granada, Spain
8. Andalusian Institute for Earth System Research (IISTA-CEAMA), Avda. del Mediterráneo s/n, 18006, Granada, Spain
9. Consiglio Nazionale delle Ricerche - Istituto di Metodologie per l Analisi Ambientale (CNR-IMAA), Potenza, Italy
10. Laboratoire d'Optique Atmosphérique, Lille, France
11. Laboratoire de Physico-chimie de l'atmosphère (LPCA), Université du Littoral Cote d'Opale, Dunkerque, France
12. Consorzio Nazionale Interuniversitario per le Scienze Fisiche della Materia, Naples, Italy
13. Dipartimento di Matematica e Fisica, Università del Salento, Lecce, Italy
14. INAF - Osservatorio Astrofisico di Catania, Italy
15. Istituto Nazionale di Geofisica e Vulcanologia, Osservatorio Etneo, Sezione di Catania, Italy
16. Dipartimento di Scienze Fisiche, Università di Napoli "Federico II", Naples, Italy
17. Consiglio Nazionale delle Ricerche – Istituto Superconduttori, Materiali Innovativi e Dispositivi (SPIN-CNR), Italy

Contact author: Rubén Barragán, ruben.barragan@tsc.upc.edu

ABSTRACT

During the ADRIMED (Aerosol Direct Radiative Impact on the regional climate in the Mediterranean region) special observation period (SOP-1a), conducted in June 2013 in the framework of the ChArMEx (Chemistry Aerosol Mediterranean Experiment) project, a moderate Saharan dust event swept the Western and Central Mediterranean Basin (WCMB) from west to east during a 9-day period between 16 and 24 June. This event was monitored from the ground by six EARLINET/ACTRIS (European Aerosol Research Lidar Network / Aerosols, Clouds, and Trace gases Research InfraStructure Network) lidar stations (Granada, Barcelona, Naples, Potenza, Lecce and Serra la Nave) and two ADRIMED/ChArMEx lidar stations specially deployed for the field campaign in Cap d'en Font and Ersa, in Minorca and Corsica Islands, respectively. The first part of the study shows the spatio-temporal monitoring of the dust event during its transport over the WCMB with ground-based lidar and co-located AERONET (Aerosol Robotic Network) Sun-photometer measurements. Dust layer optical depths, Ångström exponents, coarse mode fractions, linear particle depolarization ratios (LPDRs), dust layer heights and the

dust radiative forcing estimated in the shortwave (SW) and longwave (LW) spectral ranges at the bottom of the atmosphere (BOA) and at the top of the atmosphere (TOA) with the Global Atmospheric Model (GAME), have been used to characterize the dust event. Peak values of the AERONET aerosol optical depth (AOD) at 440 nm ranged between 0.16 in Potenza and 0.37 in Cap d'en Font. The associated Ångström exponent and coarse mode fraction mean values ranged from 0.43 to 1.26 and from 0.25 to 0.51, respectively. The mineral dust produced a negative SW direct radiative forcing at the BOA ranging from -56.9 to -3.5 Wm^{-2}. The LW radiative forcing at the BOA was positive, ranging between +0.3 and +17.7. The BOA radiative forcing estimates agree with the ones reported in the literature. At the TOA the SW forcing varied between -34.5 and +7.5 Wm^{-2}. In 7 cases the forcing at the TOA resulted positive because of the aerosol strong absorbing properties (0.83 < Single Scattering Albedo (SSA) < 0.96). The multi-intrusion aspect of the event is examined by means of air- and space-borne lidar measurements, satellite images and back-trajectories. The analysis reported in this paper underline the arrival of a second different intrusion of mineral dust observed over southern Italy at the end of the considered period which probably results in the observed heterogeneity in the dust properties.

Key words: ADRIMED, ChArMEx, AERONET, lidar, CALIOP, multi-intrusion, Saharan dust event, optical depth, radiative forcing, GAME, back-trajectories

1. Introduction

The Mediterranean region is one of the most sensitive regions to global warming according to recent climate projections (Marbà et al., 2015). The Mediterranean Basin Is located at the crossroads of air masses carrying both natural (e.g. desert particles, sea salt, volcanic ashes) and anthropogenic (e.g. black carbon, sulfate) aerosols from continental and ocean sources (Lelieveld et al., 2002). General Circulation and Regional Climate Models (GCM and RCM) show substantial variations in the hydrological cycle and a temperature increase before the end of the century in the Mediterranean region (Sánchez-Gómez et al, 2009). The Mediterranean basin represents a good place to estimate the mineral dust radiative impact (Forster et al, 2007; Mallet et al, 2016). The Mediterranean mineral dust comes, mainly, from the Sahara desert, which is the largest dust source in the world. Sahara desert emits half of the world atmospheric mineral dust (Prospero et al, 2002). During summer the strong heating of the North African regions, causes highly convective processes, which lifts large amount of dust then transported over the Atlantic Ocean, the Mediterranean Sea and Europe (Barkan et al, 2004).

The mineral dust role on the atmospheric processes is not totally known in the estimation of the Earth's energy balance (IPCC 2013). The presence of dust particles in the atmosphere over the Mediterranean Sea, increases significantly the optical depth (Mallet et al., 2016). Estimations of aerosol radiative forcing obtained with one dimensional (1D) radiative transfer models have been used to constrain and/or validate regional climate models. Many of these 1D models, widely accepted and used by the scientific community, are available as open-source codes, for example SBDART (Ricchiazzi et al., 1998) and MODTRAN (Berk et al., 2006). Such models have been used to estimate locally the aerosol radiative forcing at selected Mediterranean sites (Meloni et al., 2003; Bergamo et al., 2008; Sicard et al., 2012; 2014; Mallet et al., 2016; Romano et al., 2016; Barragan et al., 2016).

The main goal of the Chemistry-Aerosol Mediterranean Experiment (ChArMEx; http://charmex.lsce.ipsl.fr) initiative is a scientific assessment of the present and future state of the atmospheric environment in the Mediterranean Basin, and of its impact on the regional climate, air quality, and marine biogeochemistry. In the framework of ChArMEx and the Aerosol Direct Radiative Forcing on the Mediterranean Climate (ADRIMED, http://adrimed.sedoo.fr/) project (Dulac, 2014), intensive measurements of the aerosol radiative properties were carried out in the Western and Central Mediterranean basin during the summer 2013 special observation period (SOP-1a) field campaign. More details about the campaign can be found in Mallet et al., 2016. Results from the contribution of EARLINET/ACTRIS (European Aerosol Research Lidar NETwork / Aerosols, Clouds, and Trace gases Research InfraStructure Network, http://www.actris.eu/; Pappalardo et al., 2014) to the campaigns can be found in Sicard et al. (2016a). Continuous measurements of the shortwave (SW) and longwave (LW) radiative fluxes at the surface were carried out at several sites spread in the Western and Central Mediterranean Basin (WCMB) during the moderate Saharan dust outbreak that affected the Mediterranean basin from 15 to 25 June 2013 (Barragan et al., 2015). In this work, we have investigated the temporal evolution of the aerosol horizontal and vertical distribution over the WCMB during the complete event. For this purpose we have characterized the aerosol evolution using the dust regional atmospheric model BSC-DREAM8B v2.0 (Pérez et al. 2006a, Pérez et al. 2006b, Basart et al. 2012), AERONET Sun-photometer data (Aerosol Robotic Network; http://aeronet.gsfc.nasa.gov/; Holben et al., 1998), and the Spinning Enhanced Visible and Infrared Imager (SEVIRI) observations on board Meteosat Second Generation (MSG). The spatio-temporal monitoring of the evolution of the mineral dust plume during its transport over the WCMB was carried out by six ground-based lidar included in the EARLINET/ACTRIS and two ChArMEx supersites deployed specially for the SOP-1a field campaign. Co-located AERONET Sun-photometers provided the aerosol layer optical depth (AOD), Ångström exponent (AE) and coarse mode fraction. The second part of the study is focused on the radiative effect of the mineral dust outbreak estimated by the radiative transfer model GAME (Global Atmospheric Model; Dubuisson et al., 2004, 2006). In the third part the concept of multi-intrusion is investigated. We

called multi-intrusion an event which has more than one dust source. The multi-intrusion aspect of the event is further investigated using airborne lidar measurements performed from the French Falcon 20 research aircraft deployed during the field campaign, spaceborne lidar measurements from the CALIOP (Cloud-Aerosol Lidar with Orthogonal Polarization) instrument, satellite images from SEVIRI and backtrajectories.

The instrumentation and the large-scale overview of the dust event are described in Section 2. The main results related to the evolution of the mineral dust outbreak are presented and discussed in Section 3. The radiative forcing is described in Section 4. The multi-intrusion aspect of the event is discussed in Section 5. Summary and conclusions are reported in Section 6.

2. Instrumentation and large-scale overview of the dust event

2.1.Instrumentation

The data presented here were obtained at six EARLINET stations, two ChArMEx supersites equipped for documenting the aerosol properties and six co-located AERONET Sun-photometers. The characteristics of the ground-based instruments are summarized in Table 1 and the location of these instruments is represented in Figure 1 (in red the lidar stations and a yellow sun for the AERONET Sun-photometers). Most of the lidar stations considered here are equipped by Raman channels, allowing for direct extinction measurements. However this capability is typically limited to night-time conditions owing to the solar background saturates the photo-detectors of the Raman channels. For daytime observations, the dust feature AOD reported in the following is obtained using an altitude-independent lidar ratio (LR) value equal to 50 sr, at all the lidar wavelengths as typical value for desert dust (Müller et al., 2009, Mona et al., 2014).

Figure 1 shows the CALIPSO tracks (diurnal overpasses in blue and nightly overpasses in pink) during the event over the WCMB. It is interesting to notice that the overpass on 22 June crossed south Italy and the Mediterranean Sea between the Italian peninsula and Africa. This overpass might be important for the understanding of the multi-intrusion aspect of the event. Figure 1 shows the track of the flight of the French Falcon 20 research aircraft in yellow. This track corresponds to the flight of the 22 June. The French Falcon 20 aircraft was equipped with the LNG airborne lidar (Pelon et al., 2002) providing attenuated backscatter vertical profiles at three wavelengths (1064, 532 and 355 nm). The LNG lidar was mainly used in the downward-looking mode.

MSG-SEVIRI images (Figure 2) and BSC-DREAM8b model (Figure 3) were used to set the days affected by Saharan dust. The SEVIRI sensor has one high resolution channel in the visible, two visible and one near infrared channel (0.4-1.6 μm) and eight channels in the infrared (3.9-13.4 μm) (Thieuleux et al, 2005). The atmospheric variables taken into account by the BSC-DREAM8b-model are turbulent parameters in the early stage when the dust is lifted from the ground to upper levels, winds when the dust is travelling away from the sources, in addition to thermodynamic processes, rainfall, and land cover features (Pérez et al, 2006a).

2.2.Overview of the 16-24 June 2013 dust event

Saharan dust outbreaks have different scales, from continental (Lee et al., 2012) to regional-scale. The Saharan dust event studied here is included in the second type, regional scale. Figure 2 shows the spatio-temporal evolution of the mineral dust plume over the WCMB by daily AOD values at 550 nm retrieved from the MSG/SEVIRI sensor images from 15 to 24 June. The AOD values vary for this event between 0.3 (light blue areas) and 0.8 (red areas). The days in which the light blue areas reached the different stations allow identifying the first Sahara dust day at each station, which was 16 June for Granada,Cap d'en Font and Barcelona, 17 June for Ersa, 21 June for Naples, Potenza and Serra la Nave, and 22 June for Lecce. The dust plume detected during the aforementioned campaign, moved from southern Spain on 15

June (detected in Granada, located about 215 km away from the African coast and 50km away from the Mediterranean Sea (Guerrero-Rascado et al, 2008)) to south-eastern Italy on 24 June (finally detected by Serra la Nave). On June 15, the north-western Mediterranean area was under the influence of a high-pressure system, which generated a westerly to south-westerly flow over Spain and southern France, which reinforced advection of air masses from North Africa, with large concentrations of mineral dust, as shown by SEVIRI AOD (Barragan et al., 2015). A low-pressure system moved from Great Britain towards the Gulf of Biscay and then to the Iberian Peninsula between 17 and 20 of June, a negative phase of the Western Mediterranean Oscillation (WeMO) (Martin-Vide & Lopez-Bustins, 2006), forcing the winds to veer and become southerly over the northwestern Mediterranean. After 20 of June, the WeMO turns to positive phase and the low pressure system moved to the east, generating a trough located between France and Italy, and inducing a westerly flow over the north-western Mediterranean. As a result, the aerosol load travel from the Western Mediterranean Basin to the Central Basin, resulting in a decrease of the AOD values in the west between 21 and 24 of June, while these values increased over the Central Basin. Figure 2 supports previous comments since it clearly shows the transport of the dust plume over the WCMB during the studied period. AERONET and lidar measurements were not performed on 23 of June because it was a cloudy day. Note that the Near Real Time (NRT) MSG/SEVIRI images revealed that the Saharan dust reached Granada in the morning of 15 June (6:15 UTC) and that the dust plume was no longer present at the study sites in 24 June at 9:15 UTC.

3. Spatio-temporal evolution of the mineral dust outbreak

3.1.Characterization of the dusty days

The BSC-DREAM8B v2.0 model (Pérez et al. 2006a; 2006b; Basart et al. 2012) provides forecasts of the columnar dust load every six hours. This accurate model makes it possible to investigate the potential detection of a Saharan dust event at the observing stations spread over the WCMB. Figure 3 shows the model dust load (g/m2) over the Mediterranean basin and Europe from 15 to 24 June, 2013. Both Figure 2 and Figure 3 were used to identify the dusty days at the stations of Figure 1 and then reported as red boxes in Figure 4. Note that the MSG/SEVIRI data have been considered as the truth when the BSC-DREAM8B v2.0 model results were not in agreement with the corresponding satellite data.

The green areas in figure 3 agree with the light blue, yellow and red areas in figure 2. These green areas correspond to presence of dust in the atmosphere, thus both models identify the mineral dust over the same areas at same time. Comparing these figures with AERONET AOD values at 440 nm (AOD_{440}) values (table 2), in Granada the maximum value of AOD_{440} was reported during 16 of June (0.268) a day affected by mineral dust as agree the MSG/SEVIRI data. Cap d'en Font was also affected during 16 of June according to the models and it is during this day when the maximum of AOD_{440} was found in this station (0.376). Ersa started to be affected during 19 of June, the same day in which the maximum value of AOD_{440} was reported by AERONET (0.359). According to the models, the maximum value in Ersa was during 20 of June, this difference between the days can be explained because the AERONET sun-photometers measure the total atmospheric column, given greater values owing to mineral dust mixed with other atmospheric components. Potenza is a similar case than Ersa, while the maximum value of AOD_{440} retrieved by AERONET was found during 21 of June (0.16), according to the models Potenza was affected during 21 of June but to a greater extent during 22 of June. Finally in Lecce, the maximum value of AOD_{440} was 0.331 during 23 of June, both models agree with this value showing the dust load over this station during 23 of June, being 24 of June a clear day in south Italy.

3.2.Spatio-temporal evolution of columnar properties

The localization of the 8 Sun-photometers used in this study is shown in Figure 1. To study the temporal evolution of the mineral dust plume and to assess the multi-intrusion aspect of the event, AERONET products, namely AOD_{440}, Ångström

exponents (AE) calculated at the wavelength pair 440-870 nm, Single Scattering Albedo (SSA) and the coarse mode fraction at 440 nm were used. Only AERONET level 2.0 data were considered. Minimum, maximum and mean values of those parameters are given in Tables 2 and 3.

Figure 4a shows the temporal evolution of AOD_{440} and AE at all the stations. The stations are sorted from the west to the east coinciding with the main transport path of the dust plume (Figure 2). The red boxes label the dusty days at the six stations considered in this study, the blue circles indicate the AOD_{440} and the green crosses the AE. One can observe how the combination of high AOD (blue circles) values with AE (green crosses) values around and below 1 is in most of the cases inside the red rectangles. This combination of large AOD_{440} with small AE values may indicate a significant contribution of coarse mode particles to the aerosol load (Cachorro et al., 2008 and Valenzuela et al., 2015). The maximum value of $AOD_{440}$was found in Ersa on 19 of June (0.36 at 17:33 UTC) and the minimum was found in Potenza on 21 of June (0.160 at 17:03 UTC). Meloni et al (2003, 2004 and 2008) indicate AOD values at 415.6 nm of about 0.23 – 0.26 to 0.51 for moderate dust events and AOD values at 500 nm between 0.29 and 1.18 for the 1999 – 2006 period. These values will be indicative in order to compare with the AOD values obtained in this research, due to dust cases depend also on the location and the typical AOD content.

During this event, the AERONET AOD (at 440 nm) measurements range between 0.151 (Ersa, Corsica island) and 0.30 (Barcelona), indicating that the mineral dust properties are modified during the transport, for example the coarse distribution is lost by wet or dry deposition (Osada et al, 2014). The maximum of the AOD measured by the lidars inside the mineral layer is 0.36 at 532 nm in Barcelona, and the mean value of the peak days is 0.20 at 532 and 0.21 at 355 nm. According to previous studies on the same area (Meloni et al. (2003, 2004 and 2008), Mona et al. (2012) and Papayannis et al. (2009)) the event studied in the SOP-1a campaign can be classified as a moderate dust event.

Figure 5 shows the temporal evolution of the daily averaged coarse mode fraction and SSA at the six AERONET stations. It is important to recall that the mineral dust has a considerable fraction of coarse mode particles (Müller et al, 2010). Figure 5a shows clearly the difference between the Spanish stations and the Italian stations. In the Spanish stations, the coarse mode fraction reaches values of 0.56 and 0.53 on 16 and 17 of June for Granada and Cap d'en Font, respectively (AERONET measurement were not performed in Barcelona during the dusty days). 16 and 17 of June are days with confirmed presence of mineral dust in the atmosphere, so that those coarse mode fraction corresponds to dusty days. In Ersa the coarse mode fraction is almost half of the values found at the Spanish stations: the mean value for the four days is 0.26 and the highest value found in Ersa is 0.27 on 19 of June.

In Ersa the highest values of coarse mode fraction and of AOD_{440} are found on 19 June. Despite an AOD_{440} mean value similar to the AOD_{440} mean value of the Spanish stations, the coarse mode fraction is half. Despite this low value, Ersa can be consider a station with presence of dust in this period, because of the observed increase in the coarse mode fraction at that AERONET site during those days. The strange behavior found here might be due to a type of deposition of the coarse component of the dust during its transport over the Mediterranean Sea, between Cap d'en Font and Ersa (Osada et al., 2014).

The Italian stations were characterized by coarse mode fraction values higher than in Ersa in the dusty days. In fact, on 21 of June the coarse mode fraction increased up to 0.5 at Potenza and at Lecce increased up to 0.41 on 23 of June. During 22 of June the coarse mode fraction was similar at Potenza and Lecce, 0.39 and 0.33 respectively, on 24 of June the value increased to 0.41 at Lecce. During 23 of June the coarse mode fraction values decreased to values of the background conditions (0.19) at Potenza, while on 24 of June the coarse mode increased again (0.30). The higher coarse mode fraction values for Potenza and Lecce with respect to the Ersa ones was likely due to the intrusion of a second dust event, which crossed directly from Africa to south Italy.

Figure 5b shows the SSA, which represents the ratio between scattering and extinction coefficient. The lower values of SSA_{440} are observed in Granada on 17 of June (0.83) and Lecce on 22 of June (0.89). The higher values are found in Ersa on 17 and 18 of June (0.99). Some works (Valenzuela et al., 2012; Romano et al., 2016; Sicard et al., 2016b) found that the SSA exhibited a substantial increase from 440 to 675 nm on dusty days. Accordingly, the SSA mean values in the 6 Sun-photometers taken into account in this study were equal to 0.86, 0.93, 0.94, 0.95, and 0.89 at 440 nm, 0.90, 0.96, 0.96, 0.96 and 0.9 at 675 nm, and 0.92, 0.97, 0.97, 0.96, 0.89 at 1020 nm in Granada, Cap d'en Font, Ersa, Potenza and Lecce respectively on dusty days. In Lecce SSA seems independent of wavelength which, according to Russell et al. (2010), is typical of urban/industrial or mixed aerosols.

3.3.Spatio-temporal evolution of the dust plume properties

Figure 4b shows the temporal evolution of the AOD measured by the lidars, only in the mineral dust layer. The mineral dust layer bottom height was fixed at the beginning of a sudden increase of the lidar signal. A three point window went over the lidar profile, searching a sudden variation in the slope of the signal subtracting the first value from the third. When the difference between the third and the first point of the window was greater than the mean of the values inside the window, in the middle point of the window begins the mineral dust layer. This window method was applied also for the mineral dust layer top height, in order to find the end of a sudden decrease in the slope of the lidar signal. If the lidar signal increased smoothly, the window estimated the derivative of the signal in order to make more evident the height where the mineral dust layer begins or ends.In order to convert backscatter into extinction profiles, an altitude-independent LR has been assumed for all the stations and wavelengths, as representative of lidar ratio for Saharan dust particles (Muller et al., 2009, Mona et al., 2014). The percentage error that we have on altitude-independent LR in each station is directly transferred to AOD value, so the nighttime AOD is more accurate than the daytime. This is because using an altitude-dependent LR, the LR can be adjusted in noisy lidar profiles. These lidar profiles have a better signal to noise ratio in nighttime because there is no solar background, therefore with an altitude-independent LR the nighttime AOD is more accurate. The daytime profiles and the nighttime profiles had been inverted using the Klett-Fernald-Sasano (Klett, 1985) method with an altitude-independent LR of 50sr. The red boxes in this figure are the same as the red boxes in the Figure 4a. The characteristics of the mineral dust layer of the peak day for the 8 the lidar stations are summarized in Table 4.

In Figure 4b, one can see the evolution of the lidar measured AOD from the west to the east. It is worth mentioning here that respect to previous work (Sicard et al., 2016a) here the AOD series has been extended taking advantage from the availability of many aerosol backscatter profiles at the lidar stations, especially in daytime conditions. The AOD is greater in the Spanish stations, at the beginning of the event, with peak day values of 0.26, 0.37 at 532nm and 0.37 at 355 nm in Granada, Barcelona and Cap d'en Font respectively and lower in the Italian stations, with peak day values of 0.10, 0.13 and 0.22 at 532 nm and 0.11 at 355 nm for Potenza, Naples, Lecce and Serra la Nave respectively. This point is supported by the decrease of the dust coarse fraction following a west-east gradient (see Section 3.2).

The peak measurements over Granada, Barcelona, Cap d'en Font and Ersa were observed on 16 of June at 19:30UTC, 17 of June at 14:13UTC, 18 of June at 06UTC, 20 of June at 22UTC, respectively. Too few observations are available for the Italian stations (Naples, Serra la Nave, Potenza and Lecce). The distribution of the plume on 22 June could be investigated over these stations, because they provided all profiles for this day.

It is interesting to notice that the peak moment is in a different day in the Spanish stations, while in the southern Italian stations (Naples, Lecce and Serra la Nave) the peak moment is in the same day, because the data were provided just for few days. This result suggests the presence of a second event in the south of Italy during the 22 of June. Also in Figure 4b it is clear how the AOD values are greater in Naples and

Lecce than in Potenza on 22 of June, denoting an entry of mineral dust from the south. In Serra la Nave the AOD values increase during the 22 of June, as shown in Figure 4b, reaching the highest value (peak moment) in the two last measurements available (0.11 of AOD at 13:46UTC and 14:27UTC). Regarding to the Italian stations, Naples was the first in received the dust plume and had the highest lidar AOD value (a peak of 0.13 at 12:21 UTC on 22 of June). Potenza is only 150 km from Naples and the dust plume arrived there during June 22 but the lidar AOD is lower (0.06 at 08:53 UTC), however the dust plume arrived at Lecce a few hours after Potenza and the AOD increases again (0.22 at 13:22 UTC and 0.1037 at 09:46). It is clear that a new moderate intrusion of Saharan dust joined to the first during the morning of 22 of June. During June 22, in Potenza, appeared a layer between 3-6km since the first hours of the day, and then a new layer appeared at about 11UTC at lower altitudes, supporting the arrival of a second event. The bottom height of the aerosol layer (bottom height in Table 4) varies in time. These bottom heights were retrieved by the lidar measurements. At the peak moments (Figure 6) this height is maximum in Serra la Nave (4010 m), and minimum in Cap d'en Font (201 m). Between Barcelona and Granada there is almost 1 km of difference (912 and 1719 m respectively), and Lecce has a similar difference with Potenza and Naples (809, 1630 and 1468 m respectively). These differences could be explained by the different hours of the peak moments but the mean values of the bottom height of the aerosol layer show the same behaviour (2259, 1242, 141, 2462, 1755, 1726, 1241, 4288 m for Granada, Barcelona, Cap d'en Font, Ersa, Potenza, Naples, Lecce and Serra la Nave respectively). Therefore, the explanation is that the base of the mineral dust layer is near the boundary layer, which changes with the time and with the atmospheric conditions at each station. The top height of the mineral dust layer is more constant and suffer less these variations, the mean values are 5339, 5811, 5458, 4948, 5515, 5408, 5756, 6928 m for Granada, Barcelona, Cap d'en Font, Ersa, Potenza, Naples, Lecce and Serra la Nave respectively because these top heights are located in a stable layer of the atmosphere.

Figure 6 shows the temporal evolution of the characteristics commented above of the mineral dust layers. Notice that the thickness (purple line) decreased from Barcelona and Cap d'en Font to Ersa and Potenza, while in Naples and Lecce the thickness increased again becoming similar to the Spanish stations; this again makes evident the effect of the second event.

Figure 7 shows the lidar backscatter profiles of the most characteristics days of the event in each station. One can observe how the curves which represent the backscatter profile have values greater than zero in the eight stations above 2 km. This behaviour confirms the presence of aerosol in the measurements. These aerosol structures are located between the bottom and top heights estimated in the peak moments of the event (see table 4).

Products as the linear particle depolarization ratio (LPDR) retrieved from the lidar measurements and for the most characteristic days are shown in Figure 8. It is important here the LPDR, which is an indicator of non-spherical particles (Burton et al. 2015), and assumed typical dust values around 0.3 (Tafuro et al. 2006, Mamouri et al. 2016). For the stations where the LPDR is available (Granada, Cap d'en Font, Ersa, Naples, Potenza, Lecce and Serra la Nave) the value is about 0.3 at altitude ranges identified as dust affected regions, confirming the presence of Saharan dust.

The altitude ranges in which the LPDR is about 0.3, match with the altitude range with backscatter values greater than 0 mm^{-1} sr^{-1}. Therefore, the backscatter profiles shown in figure 7 confirm the presence of Saharan dust in the eight stations.

4. Dust direct radiative forcing

4.1.The GAME radiative transfer model

The GAME Radiative Transfer Model has been used to estimate the SW and LW radiative fluxes with and without aerosol and to determine the aerosol direct radiative forcing (DRF) at the BOA and at the TOA. The aerosol DRF represents the changes undergone by the radiation due to the presence of aerosol and is defined as the difference between the net fluxes with and without aerosol:

$$DRF_{BOA} = (F_{BOA}^{DN} - F_{BOA}^{UP}) - (F_{BOA}^{DN,0} - F_{BOA}^{UP,0})$$

$$\begin{aligned} DRF_{TOA} &= (F_{TOA}^{DN} - F_{TOA}^{UP}) - (F_{TOA}^{DN,0} - F_{TOA}^{UP,0}) \\ &= F_{TOA}^{UP,0} - F_{TOA}^{UP} \end{aligned}$$

where F^{DN} and F^{UP} are the downward and upward fluxes with aerosol, while $F^{DN,0}$ and $F^{UP,0}$ are the downward and upward fluxes without aerosol, respectively.

The GAME code is widely described by Dubuisson et al. (2004, 2006) and recently in the LW spectral range by Sicard et al. (2014). GAME allows calculating the solar and thermal infrared fluxes in two adjustable spectral ranges: shortwave (0.3-4 μm) and longwave (4-37 μm), at the boundary of plane and homogenous atmospheric layers by using the Discrete Ordinates Method (DISORT) (Stamnes et al., 1988). 40 vertical levels are used, in the LW version, between ground and 100 km height with a resolution of 1 km from the surface to 25 km, 2.5 km between 25 and 50 km, 5 km from 50 to 60 km, and 20 km between 80 and 100 km. In the SW version, 18 vertical levels are used between ground and 20 km height with a resolution of 5 meters from the surface to 10 meters, 10 meters between 10 and 50 meters, 50 meters between 50 and 100 meters, 100 meters between 100 and 200 meters, 200 meters between 200 and 1 km, 1 km between 1 and 2 km, 2 km between 2 and 10 km and 10 km between 10 and 20 km. One of its main specificities is the representation of the LW aerosol scattering, which is often neglected in regional and global climate models in spite of its effect on the LW radiative forcing (Sicard et al., 2014). Table 5 provides the list of the main parameters used as inputs of GAME in the SW and LW spectral range, the aerosol optical properties, including asymmetry factor, are introduced as inputs in the model. Other studies like Guleria and Kuniyal (2016) and Koepke et al. (2015) show the utility of models to get the optical parameters in order to estimate the aerosol radiative forcing, concretely the Optical Properties of Aerosol and Cloud (OPAC) model (Hess et al., 1998). In this research we preferred to use the AERONET data because the AERONET sun-photometers provide these parameters directly and all the stations of this study have an AERONET sun-photometer. The AOD, asymmetry factor and SSA from AERONET or estimated by Mie calculation are interpolated in the whole atmospheric column, applying the estimated values are used in the heights where the lidar systems detected aerosol, while in the remaining heights standard values retrieved from clear-sky days are used. The refractive index estimated by Krekov (1993) is used directly in the Mie calculation.

4.2.Dust direct radiative forcing

In this Section, we present and analyse the model-based aerosol SW- and LW-DRF values estimated during the Saharan dust event that affected the western and central Mediterranean Basin on June 2013. Mean values are summarized in Table 6. A negative or positive sign of the aerosol DRF determines whether the aerosols produce a cooling or a heating effect (Seinfeld and Pandis, 1998).

The aerosol radiative forcing is estimated for 12 cases in thre different places (Granada, Cap d'en Font and Lecce) affected by the studied event. All cases are documented by lidar profiles, radiosoundings and CERES SSF Level2 products.

The AOD varies between 0.06 (Granada 17 of June at 12:00UTC) and 0.37 (Cap d'en Font 17 of June at 12:00UTC). In general, the AERONET-derived SSA is higher than 0.9 (in 7 of the cases), but in five cases the SSA values are lower than 0.9 (0.87, 0.87, 0.83, 0.85, 0.89). These cases correspond to the presence of mineral dust with strong absorbing properties (Sicard et al., 2012; 2014).

The SW and LW DRFs calculated by GAME at the bottom of the atmosphere (BOA) and top of the atmosphere (TOA) are given in Table 6 and Figures 9 and 10.,

Figure 9 shows the temporal evolution of the SW DRF in each station. In general, the impact of the radiative forcing due to mineral dust is greater when the AOD values are high. It is clear the effect of the aerosols in the DRF, for example, at the BOA (Figure 9a), the SW DRF has always a cooling effect and varies between -3.49 W m^{-2} and -45.3 W m^{-2} in Cap d'en Font, reaching -42.3 W m^{-2} in Granada or -37 W m^{-2} in Lecce. Focusing on Cap d'en Font (triangles) during 16 and 17 of June (days with aerosol presence as is shown in figures 2 and 3) there is a cooling effect due to the aerosols. During 18 and 19 of June, where the aerosol load is lower (see AOD in Table 6) the cooling effect is lower than the previous days but is still present. Finally during 20 of June in Cap d'en Font, a day free of mineral dust, according to Figures 2 and 3, the SW DRF at BOA is -3.49 Wm^{-2}, while the SW DRF at BOA values for 16 and 17 of June are -45.3 W m^{-2} and -44.9 W m^{-2} respectively. the LW DRF (figure 9b) has always a heating effect and varies between +0.26 W m^{-2} (Naples) and +17.7 W m^{-2} (Cap d'en Font). These results are consistent with the radiative forcing (RF) estimated by Sicard et al. (2014). In table 6, also, are showed the Radiative Forcing values estimated by AERONET.

At the TOA, the SW DRF has a cooling effect in 7 of the cases and a heating effect in 5 cases (Table 6 and Figure 10a). The 5 heating cases in this study are cases with low values of SSA. By comparing those results with other studies like Dubovik et al. (2002), Sicard et al. (2012; 2014) or Barragan et al. (2016) one can conclude that the strong absorbing properties may be due to a mixing of dust with polluted aerosols. Concretely in Sicard et al. (2014) only on 22 of July 2009 the TOA SW RF was positive (+8.5 W m^{-2}) for AERONET SSA_{440} = 0.83 and SZA = 21.1°. The low values of SSA_{440} and solar zenith angle (SZA) were responsible of positive value of the TOA SW RF. Also, Sicard et al. (2014) found that the SSA_{440} reached a smaller value of 0.79 on 21 of July 2009. Nevertheless, they found that the TOA SW RF value was negative (-22.8 W m^{-2}) and SZA = 77°. The larger SZA value was responsible for the negative sign of the TOA SW RF. Finally, studies like Seinfeld and Pandis (1998) suggest that the heating effect at TOA in the SW might be due to the aerosol backscatter fraction, which increases with the SZA and Liao and Seinfeld (1998) found for a uniform aerosol layer (from the Earth's surface to 5 km) made of pure ammonium sulfate, pure soot, internal mixture, and external mixture, positive TOA SW RF at SZA = 0°.The internal and external mixtures were also responsible for positive TOA SW RF. One can deduce that the positive TOA SW RF values were associated with small values of SSA and SZAs, which is the case of Naples on 22 of June. The LW RF (Table 6 and Figure 10b) varies between 0.34 and 8.96 W m^{-2}, all the cases have a heating effect (positive values) and match with the results found in previous studies. The SW AERONET Radiative Forcing (ARF) at TOA, ranges between -6 (Lecce) and -15.3 (Granada), has a cooling effect in all the cases and in general the cooling effect is greater than the effect of the DRF. This behaviour can be explained because the DRF is estimated only in the dust layer while the ARF is estimated for the total atmospheric column observed by the sun-photometers. In the cases where the AOD retrieved from lidar measurements confirms the presence of mineral dust in the atmosphere, the ARF and DRF values are similar. At BOA, the ARF ramges between -14.7 (Cap d'en Font) and -42.6 (Granada) and has a cooling effect for all the cases, as at TOA. At BOA the DRF has greater cooling effect than the ARF in the cases in which the AOD retrieved from lidar measurements is high. This situation can be explained thanks to the way in which the DRF is estimated, taking in account only the mineral dust which has a strong cooling effect while in the ARF are taking in account al the aerosols in the atmosphere. In figure 9a and 10a the big differences found in Barcelona are due to the different AOD values found during the 17 of June (see table 6).

The Lecce behaviour of the aerosol DRF is also interesting (Figure 9a). This station was affected by the mineral dust outbreak on 21, 22 and 23 of June and have low values of AOD compared to the Spanish stations. These data lead to cooling effects

lower (in absolute terms) than the previous sites, except for the 22 of June where Lecce suffers a strong cooling effect (-37 W m^{-2}) comparable with the DRF estimated in the Spanish stations. This coolig effect may be due to the increase of the AOD, in2 times in Lecce, compared to the previous days in this Italian station. This result supports the theory of a new mineral dust outbreak which reaches south Italy directly from Africa,

Figure 9b shows the temporal evolution of the LW DRF at BOA; the behaviour is similar to the SW RF at BOA but with opposite sign (heating effect). In cases where the AOD values measured by the lidars are small the RF values is near to zero; for example, in Granada on 17 of June, a day without mineral dust in the atmosphere, for an AOD = 0.06, the DRF was +0.27 W m^{-2}. Here again the results in the Italian station of Lecce on 22 June are especially interesting: the LW DRF at BOA is +3.8 W m^{-2}. In this station the RF was lower in the previous days (+1.9 W m^{-2} and +1.5 W m^{-2} for Lecce on 20 and 21 of June). The second event crossed the Italian peninsula from the south.

5. Multi-intrusion aspect of the Saharan dust event

Figure 11 shows the presence of two different dust events crossing the WCMB detected in four CALIPSO overpasses. Nowottnick et al. (2015) summarized attenuated backscatter values for different particles present in the atmosphere (see their Table 1); for the case of dust the attenuated backscatter is less than $5*10^{-4}$ (pink values in the Figure 11 scale), therefore the red areas in Figure 11 can be considered as mineral dust. Nowottnick et al. (2015) also indicate that the depolarization ratio value for the mineral dust is less than 0.20 in the CALIPSO measurements. The first overpass was diurnal on 20 of June; in this one only the first event is detected reaching Italy. On the second overpass on the night of 20-21 June the second event (the red and yellow area) is detected still in North Africa. During the overpass on the night of 21-22 June the two events are over the Italian peninsula. In this overpass the depolarization ratio is available, the yellow-green area selected as the second event, has the correct values for mineral dust in the attenuated backscatter and in the depolarization ratio images.

Figure 12 shows the French Falcon 20 flight on 22 of June. The stations of Serra la Nave, Lecce and Naples are marked in white in the figure and the red areas correspond to the mineral dust layers. The red areas correspond to mineral dust presence and the yellow areas correspond to clouds. One can observe a red area between 4 and 6 kilometers which reach Serra la Nave at 11:30UTC, approximately and came from the Gulf of Sidra (North Africa). The rest of the mineral dust showed in the figure is located between the ground and 4 kilometers and was detected over south Italy (Serra la Nave, Lecce and Naples). Therefore, it is clear that the Falcon 20 detected the second event during the first hour of the flight (between 10:27 and 11:30UTC).

Figure 13 show several 72-hours back-trajectories with origin in different stations. These back-trajectories were obtained from the HYSPLIT model (Stein et al, 2015). The heights selected at the origins of the back-trajectories correspond to the heights of the aerosol layers detected by the lidars (see Section 3.3). Figure 13a1 shows a back-trajectory with end in Granada and it is clear that the origin of the dust is North Morocco and Algeria. The origin of the dust detected in Barcelona (Figure 13a2) was the same than that of the dust detected in Granada: in both stations the same event was detected. The green line in Figure 13a2, the higher back-trajectory, reached Barcelona directly from Granada, while the red and blue lines crossed the sea.

Figure 13b shows the origin of the dust which affected Cap d'en Font in the four days with presence of mineral dust confirmed by the method explained in the section 3.1. Figure 13b1 shows that the origin of the dust is the Iberian Peninsula: the same dust that reached Granada travelled from this city in the South of Spain to Cap d'en Font on 16 of June. Figure 13b2 shows the same origin of the dust on 17 June as for Granada and Barcelona at the three heights: North Morocco and Algeria. Figure 13b3

shows that the origin of the dust on 18 of June is Algeria at all the heights, no back-trajectory came from the Iberian Peninsula. The spatial evolution of the dust plume, from the west to the east, became evident in these back-trajectories. Figure 13b4 shows that for the 19 of June the origin for the higher back-trajectories was North Africa again, but the lower back-trajectory came from the Iberian Peninsula.

Figure 13c shows a back-trajectory for the 19 of June at 12:00UTC, the same day and the same hour than Figure 13b4 but the origin now is the station of Ersa. The air masses reaching Ersa passed over North Algeria and the lower air mass crossed Tunisia. This back-trajectory explained the behaviour of the back-trajectory shown in Figure 13b4; the strong component of the Saharan dust event was out of Cap d'en Font during 19 of June and was entering in the area of Ersa (see Figure 2).

Figure 13d shows the origin of the dust during the 22 of June, the day that the second event reached South Italy, for the Italian peninsular stations. Figure 13d1, with origin in Naples, corresponds to the morning of the 22 of June (9:00UTC); at this time the second event had not yet reached the South of Italy and the air masses came from North Algeria. Figure 13d2 shows the back-trajectories of the air masses that arrived to Potenza on 22 of June at 23:00UTC; at this time the second event was present over South Italy and is the air masses come no longer from North Algeria, but since 22 of June at noon thy come from Tunisia. This idea is confirmed in Figure 13d3, which shows the air masses which passed over Potenza and arrived in Lecce on 22 of June at 12:00UTC. The origin of these air masses was Tunisia, thereby confirming the presence of a second dust event with a different origin than the first one.

Figure 13d4 shows the back-trajectories modelled for Serra la Nave during 22 of June. The highest air masses (green and blue lines), which correspond to the air masses with aerosol presence (see Section 3.3 and bottom and top heights in Table 4), have the same origin in Tunisia as the back-trajectories of the Figure 13d2 and Figure 13d3.

Figure 14 shows several particle position plots simulated by HYSPLIT. The heights selected, from 0 to 6000 m, correspond to the heights at which the dust is detected in the stations. Figure 14a1 shows a 72 hours particle position plot with end in Granada and it is clear that the particles during these three days travelled from North Africa to the South of the Iberian Peninsula, with origin in North Morocco and Algeria, as one can see in figure 13a1. Figure 14a2 shows the same simulation as in the previous figure but now the end is located in Barcelona: the origin of the dust is the same as in the figure 14a1 but now the particles were sparse over the Mediterranean between Italy and Spain. This explains why in Cap d'en Font the dust was detected at the same time than in the peninsula. The back-trajectories reaching Barcelona directly from Granada (Fig. 13a2 and 14a2) shows that the event detected in Granada and Barcelona stations was the same.

Figure 14b shows the origin of the dust which affected Cap d'en Font from 16 to 19 June. Figure 14b1 shows that dust covered the south and east of the Iberian Peninsula. Figure 14a2 confirms that the dust transported over Granada on 16 June reaches Cap d'en Font on 17 June, and how the dust was still present over North Africa during 17 June. Figure 14b3 shows that the origin of the dust on 18 June is in Algeria, and that the dust covers the whole southwestern Mediterranean basin. It is evident that the origin of the dust during these days was Algeria. Figure 14b4 shows that on 19 June the dust present in lowest layers had its origin in Tunisia, while the dust present in the highest layers had its origin in Tunisia.

Figure 14c shows a particle position plot for the 19 of June at 08:00UTC, the same day and the same hour than Figure 14b4 but arriving at the station of Ersa. The origin of the particles was still North Africa but the particles detected in Ersa crossed Cap d'en Font before, therefore the same dust which reached Cap d'en Font, travelled to the north and reached Ersa.

Figure 14d shows the particle position on 22 June, which end in the three Italian peninsular stations. Figure 14d1, with end in Naples, corresponds to the morning of the 22 of June (08:00UTC), one can observe how the tail of the event was over Algeria, while in the lowest layers (black areas) the dust was starting to accumulate from Tunisia. Figure 14d2 shows the particle position with end in Potenza on 22 of June at 08:00UTC, the second event was present in the black areas and the tail of the higher layers was still coming from Algeria, but crossing Tunisia before reaching South Italy. Figure 14d3 shows the air masses arriving in Lecce on 22 of June at 08:00UTC: the origin was clearly Tunisia, while the tail was no longer crossing Morocco and Algeria, which confirm the presence of two different Saharan dust events with different origins.

Figure 14d4 shows the particle position plot modelled for Serra la Nave on 22 June at 23:00UTC. The clear blue areas evidence that the dust had its origin in Tunisia.

6. Summary and Conclusions

The spatio-temporal evolution of mineral dust vertical profiles and optical properties and the dust direct radiative forcings in the SW and LW spectral ranges at BOA and TOA have been determined and analyzed for a moderate Sahara dust event over the western and central Mediterranean Basin. The products as SSA and AOD_{440} retrieved from the AERONET Sun-photometers CALIOP attenuated backscatter profiles from the CALIPSO satellite, the MSG/SEVIRI daily AOD images from METEOSAT and the modelled products as coarse mode fraction estimated from the AERONET Sun-photometers data, the mineral dust layer properties extracted from the lidar signals, the HYSPLIT back-trajectories and the radiative forcings at the TOA and at the surface modelled by GAME, have been analysed while during the 16-24 June 2013 Saharan dust outbreak that affected the WCMB. Several relevant results were found:

- A moderate Saharan dust event swept the Western and Central Mediterranean Basin from 16 June to 24 June, affecting directly to eight stations spread over the WCMB.

- For this moderate event, we found that travelling over Mediterranean Basin the dust layer geometrical and optical properties changed in the west-east direction: dust particles reached higher altitude over Italy while the columnar AOD was higher over Spain with correspondingly higher presence of coarse particles.

- The AOD measured by the AERONET Sun-photometer and retrieved from the lidar measurements is greater in the Spanish stations and lower in the Italian stations. The increase of the AOD retrieved by lidar measurements and the AOD from AERONET observations during 22 June in Naples and Lecce denote the entry of a second Saharan dust event that only reached the southern Italian stations. Products as the Ångström exponent at 440–870 nm and the AOD_{440} undergo a sharp SW–NE gradient between the Spanish stations and Ersa one. The dust coarse mode fraction decreases following a west-east gradient like the AOD. Again, during 22 June the coarse mode fraction increases, like the AOD. The temporal behavior of AOD and coarse mode fraction over the Italian stations suggests the entry of a second Saharan dust event which only reached the southern Italian stations. Hypothesis confirmed by a detailed analysis of CALIPSO and airborne lidar observations collected during the investigated period in the study area. Lower values of SSA that affected the results of the SW radiative forcings at TOA were found and pointed out the presence of aerosols with strong absorbing properties.

- By using a typical LR of 50sr for the daytime lidar measurements and the extinction profiles for the nighttime measurements, the obtained profiles were coherent and allowed to extract the mineral layer bottom and top heights and the mineral layer AOD with optimal results. The bottom heights were extremely variable ranging in values lower than 1 km (911 m in Barcelona, 201 in Cap d'en Font and 809 m in Lecce) to 4 km (4010 m) in Serra la Nave. This behaviour can be explained by the orography of the different areas and the location of the lidar station (see table 1). The top heights range between 5 km (Granada, Ersa and

Potenza) and 7 km (Naples and Serra la Nave). The three Italian stations affected by the second event present the highest values of top heights (6790 m in Lecce, 7708 m in Naples and 7910 m in Serra la Nave), which are similar to the value found in Barcelona (6584 m). In this case the orography is not as important as in the bottom heights and the behaviour of the top height in the Italian stations may be due to particles located in higher air masses, which compose the second event. Accordingly the thickness of the aerosol layer at the peak moment is greater in Barcelona (5672 m), Naples (6240 m) and Lecce (5981 m), being Barcelona the station were the first event affected most and Naples and Lecce stations affected by the second event (see table 4).

- The LPDR (figure 8) values in the stations affected by the first event were ranging between 0.21 and 0.27 in Granada, 0.24 and 0.39 in Cap d'en Font, and 0.18 and 0.21 in Ersa. The stations affected by both events present LPDR values which range between 0.21 and 0.32 in Naples, 0.26 and 0.31 in Potenza, 0.22 and 0.25 in Lecce and 0.21 and 0.25 in Serra la Nave. The values in all the stations are around 0.3 (the assumed typical dust value). In most of the cases the LPDR values are lower than 0.3, which indicates that the dust was mixed with humidity (for example, fog and cloud droplets are totally polarizing particles, so its LPDR value is around 0) and air pollutants.

- The temporal evolution of the radiative forcing estimations from west to east correlates with the loss of the coarse mode during the first Saharan dust event. The beginning of the second event (22 June) at Naples and Lecce, corresponds to radiative forcing similar to what found in the intense case of the first dust event observed at Spanish stations.

- Negative values where found for the 18 studied cases, therefore cooling effect of the aerosols, in the SW range at the BOA. These values range between -7 W m^{-2} in Lecce on 24 June, day without mineral dust in the atmosphere, and -45.3 W m^{-2} in Cap d'en Font on 16 June, a dusty day. Further at BOA, the LW radiative forcings present positive values (heating effect of the aerosols), these values vary between +0.3 W m^{-2} in Granada during 17 June (dusty day) and +17.7 in Cap d'en Font on 17 June. This LW radiative forcing at BOA is very high compared with the results found in the literature for dusty days and might be due to the extremely high AOD measured (0.37). In general, the modelled SW and LW radiative forcings SW at BOA agree with the results found in the literature.

- On the other hand, the SW radiative forcings modelled at TOA range between -34.5 W m^{-2} in Cap d'en Font (16 June) and +5.8 W m^{-2} in Granada (16 of June). In total 5 cases (41.7%) show positive SW radiative forcings at TOA, contradicting the literature. These positive SW forcings are associated with low values of SSA, and SZA. The dust contamination by anthropogenic particles during its transport was likely responsible of the increase of the light absorbing properties by aerosol particles and, hence, for the decrease of the SSA values.

- Finally at TOA, the LW radiative forcings present positive values, which range between +0.2 in Granada (17 June) and +8.9 in Cap d'en Font (19 June) in agreement with the literature.

- The strong phase of the 2 detected events had the same effect on the radiation budget, with values of -36.9 (BOA SW), +6.3 (BOA LW), +5.8 (TOA SW) and +7.0 W m^{-2}(TOA LW) over Granada, 16 June, and of -37 (BOA SW), +3.8 (BOA LW), +4.3 (TOA SW) and 2.4 (TOA LW) W m^{-2} for Lecce on 22 June.

- The CALIPSO overpasses show clearly the presence of two different mineral dust events which affected the Italian Peninsula during 22 June. Further insight on this temporal evolution is provided by HYSPLIT back-trajectories analysis, which clearly shows two different origins for the air masses that carried the Saharan dust which affected Spain and Italy during the same week. The first days of the event (from 16 to 20 June) the dust affected the Spanish stations (Granada, Barcelona and Cap d'en Font) and Ersa, and came from Morocco and North

Algeria, while during 22 and thereafter the origin of the mineral dust detected by some of the participating stations were Tunisia. Two different origins suggest two different events in a short period of time. The particle position plots show similar results as the back-trajectories and confirm that the dust detected in Barcelona and Cap d'en Font was transported directly from Granada during the first days of the event. The dust detected in Ersa was previously transported over Cap d'en Font. The particle position plots in Naples and Potenza these stations were affected only by the tail of this first dust event with particles originated in Algeria. Finally in Lecce and Serra la Nave the particles reached the stations directly from Tunisia. Therefore the presence of two different events is confirmed using two different HYSPLIT methods.

In conclusion, the results discussed in this paper can be considered of interest because they refer to the multi-intrusion aspect of a Saharan dust outbreak, a dust event scenario poorly investigated. It is also interesting to note the large area under study and the huge amount of data analyzed to gain a better understanding of the behaviour of the Saharan dust events at a regional level over the Mediterranean basin.

Acknowledgments

This study is performed in the framework of workpackage 4 on aerosol-radiation-climate interactions of the coordinated program ChArMEx (the Chemistry-Aerosol Mediterranean Experiment; http://charmex.lsce.ipsl.fr). It is also supported by the ACTRIS (Aerosols, Clouds, and Trace Gases Research Infrastructure Network) Research Infrastructure Project funded by the European Union's Horizon 2020 research and innovation programme under grant agreement n. 654169 and previously under grant agreement n. 262254 in the 7th Framework Programme (FP7/2007-2013); by the Spanish Ministry of Economy and Competitivity (project TEC2012-34575 and TEC2015-63832-P) and of Science and Innovation (project UNPC10-4E-442) and EFRD (European Fund for Regional Development); by the Department of Economy and Knowledge of the Catalan autonomous government (grant 2014 SGR 583); and by the Andalusia Regional Government through projects P12-RNM-2409 and P10-RNM-6299. This work was funded by the VAMOS SEGURO project, Programma di Cooperazione Transfrontaliera Italia-Malta 2007–2013, A1.2.3-62, Obiettivo Specifico 2.3. ChArMEx-France is supported through the MISTRALS program by INSU, ADEME, Météo-France, and CEA. ADRIMED project was mainly supported by the French Agence Nationale de la Recherche. AERONET/PHOTONS is acknowledged for calibration of the Ersa Sun-photometer. Acknowledgement to AERONET for sunphotometer quality-assured data processing and distribution.

References

Armenante M, Boselli A, Nasti L, Pica G, Spinelli N, Wang X (2004) Atmospheric aerosol characterization in the urban area of Napoli. Combustion Colloquia 2009, Proceedings of SPIE - The International Society for Optical Engineering5235, doi: 10.1117/12.514247.

Barkan J, Kutiel H, Alpert P, Kishcha P (2004) Synoptics of dust intrusion days from the African continent into the Atlantic Ocean, J. Geophys. Res., 109, D08201, doi: 10.1029/2003JD004416.

Barragan R, Sicard M, Totems J, Léon JF, Renard JB, Dulac F, Mallet M, Pelon J, Alados-Arboledas L, Amodeo A, Augustin P, Boselli A, Bravo-Aranda JA, Burlizzi P, Chazette P, Comerón A, D'Amico G, Granados-Muñoz M J¸ Leto G, Guerrero-Rascado JL, Madonna F, Mona L, Muñoz-Porcar C, Pappalardo G, Perrone MR, Pont V, Rocadenbosch F, Rodriguez A, Scollo S, Spinelli N, Titos G, Wang X, Zanmar Sanchez R (2015) Characterization of Saharan dust ageing over the western Mediterranean Basin during a multi-intrusion event in June 2013 in the framework of the ADRIMED/

ChArMEx campaign, EGU General Assembly, Vienna, Austria, 12-17 April 2015, Geophysical Research Abstracts, Vol. 17, EGU2015-2789.

Barragan R, Romano S, Sicard M, Burlizzi, P, Perrone MR, Comeron A (2016) Estimation of mineral dust direct radiative forcing at the EARLINET site of Lecce, Italy, during the ChArMEx/ADRIMED summer 2013 campaign: impact of radiative transfer model spectral resolutions, J. Geophys. Res., 121, doi: 10.1002/2016JD025016.

Basart S, Pérez C, Nickovic S, Cuevas E, Baldasano JM, (2012) Development and evaluation of the BSC-DREAM8b dust regional model over Northern Africa, the Mediterranean and the Middle East. Tellus B, 64, 1-23.

Bergamo A, Tafuro M, Kinne S, De Tomasi F, Perrone MR(2008) Monthly-averaged anthropogenic aerosol direct radiative forcing over the Mediterranean from AERONET derived aerosol properties, Atmos. Chem. Phys., 8, 6995-7014.

Berk A, Anderson GP, Acharya PK, Bernstein LS, Muratov L, Lee J, Fox M, Adler-Golden SM, Chetwynd JH, Hoke ML, Lockwood RB, Gardner JA, Cooley TW, Borel CC, Lewis PE, Shettle EP (2006) MODTRAN5: 2006 Update, Proc. SPIE, Vol. 6233, 62331F.

Bösenberg J, Ansmann A, Baldasano JM, Balis D, Böckmann C, Calpini B, Chaikovsky A, Flamant P, Hagard A, Mitev V, Papayannis A, Pelon J, Resendes D, Schneider J, Spinelli N, Trickl T, Vaughan G, Visconti G, Wiegner M (2001) EARLINET: a European aerosol research lidar network, laser remote sensing of the atmosphere. In: Dabas A, Loth C, Pelon J (Eds.), Selected Papers of the 20th International Laser Radar Conference, 2001. Edition Ecole Polytechnique, Palaiseau, France, pp. 155–158.

Burton SP, Hair JW, Kahnert M, Ferrare RA, Hostetler CA, Cook AL, Harper DB, Berkoff TA, Seaman ST, Collins JE, Fenn MA, Rogers RR (2015) Obervations of the spectral dependence of linear particle depolarization ratio of aerosols using NASA Langley airborne High Spectral Resolution Lidar, Atmos. Chem. Phys. , 15, 13453–13473, doi: 10.5194/acp-15-13453-2015.

Cachorro VE, Toledano C, Prats N, Sorribas M, Mogo S, Berjón A, Torres B, Rodrigo R, de la Rosa J, de Frutos AM (2008) The strongest desert dust intrusión mixed with smoke over the iberian Peninsula registered with Sun photometry, J. Geophys. Res., 113, D14S04.

Chazette P, Totems J, Ancellet G, Pelon J, Sicard M (2016) Temporal consistency of lidar observations during aerosol transport event in the framework of the ChArMEx/ ADRIMED campaign at Minorca in June 2013. Atmos. Chem. Phys., 16, 2862-2875, doi: 10.5194/acp-16-2863-2016.

Dubovik O, Holben B, Eck T, Smirnov A, Kaufman Y, King M, Tanré D, Slutsker I (2002) Variability of Absorption and Optical Properties of Key Aerosol Types Observed in Worldwide Locations, J. Atmos. Sci. 59, 590–608.

Dubuisson P, Dessailly D, Vesperini M, Frouin R (2004) Water Vapor Retrieval Over Ocean Using Near-Infrared Radiometry, J. Geophys. Res., 109, D19106, doi: 10.1029/2004JD004516.

Dubuisson P, Roger J, Mallet M, Dubovik O (2006) A Code to Compute the Direct Solar Radiative Forcing: Application to Anthropogenic Aerosols during the Escompte Experiment, Proc. International Radiation Symposium (IRS 2004) on Current Problems in Atmospheric Radiation, edited by: Fischer H, Sohn B-J, Deepak A, Hampton, 127–130, 23–28 August 2004, Busan, Korea.

Dulac F (2014) An overview of the Chemistry-Aerosol Mediterranean Experiment (ChArMEx), European Geosciences Union General Assembly, Geophysical Research Abstracts Vol. 16, EGU2014-11441, Vienna (Austria).

Forster P, Ramaswamy V, Artaxo P, Berntsen T, Betts R, Fahey DW, Haywood J, Lean J, Lowe D C, Myhre G, Nganga J, Prinn R, Raga G, Schulz M, Van Dor land R (2007)

Changes in atmospheric constituents and in radiative forcing, in: Climate Change 2007, The Physical Science Basis, Contribution of Working Group I to the Fourth Assessment Report of the Intergovernmental Panel on Climate Change, edited by: Solomon S, Qin D, Manning M, Chen Z, Marquis M, Averyt KB, Tignor M, Miller HL, Cambridge Univ. Press, Cambridge, UK, 129–234.

Guerrero-Rascado J L, Ruiz B, Alados-Arboledas L (2008) Multispectral lidar characterization of the vertical structure of Saharan dust aerosol over southern Spain, Atmos. Environ., 42, 2668– 2681.

Guleria RP, Kuniyal JC (2016) Characteristics of atmospheric aerosol particles and their role in aerosol radiative forcing over the northwestern Indian Himalaya in particular and over India in general, Air Qual Atmos Health 9: 795. doi:10.1007/s11869-015-0381-0.

Hess M, Koepke P, Schult I (1998) Optical Properties of Aerosols and Clouds: The software package OPAC, Bull. Am. Met. Soc., 79, 831-844.

Holben BN, Eck TF, Slutsker I, Tanre D, Buis JP, Setzer A, Vermote E, Reagan JA, Kaufman YJ, Nakajima T, Lavenu F, Jankowiak I, Smirnov A (1998) Aeronet a federated instrument network and data archieve for aerosol characterization. Remote Sensing of Environment, 66, pp. 1–19.

IPCC: Climate Change 2013: The Physical Science Basis, Contribution of Working Group I to the UN IPCC's Fifth Assessment Report (2013), Cambridge University Press, New York (USA).

Klett J D (1985) Stable analytical inversion solution for processing lidar returns, Appl. Opt. 20, 211–220.

Koepke P, Gasteiger J, Hess M (2015) Technical note: Optical properties of desert aerosol with non-spherical mineral particles: data incorporated to OPAC, Atmos. Chem. Phys., 15, 5947–5956, doi:10.5194/acp-15-5947-2015.

Krekov GM (1993) Models of atmospheric aerosols, edited by: Jennings, S. G., Aerosol Effects on Climate, University of Arizona Press, Tucson, AZ, 9–72.

Lelieveld J, Berresheim H, Borrmann S, Crutzen PJ, Dentener FJ, Fischer H, Feichter J, Flatau PJ, Heland J, Holzinger R, Korrmann R, Lawrence MG, Levin Z, Markowicz KM, Mihalopoulos N, Minikin A, Ramanathan V, de Reus M, Roelofs GJ, Scheeren HA, Sciare J, Schlager H, Schultz M, Siegmund P, Steil B, Stephanou EG, Stier P, Traub M, Warneke C, Williams J, Ziereis H (2002) Global air pollution crossroads over the Mediterranean, Science, 298, 794–799.

Leon JF, Augustin P, Mallet M, Bourrianne T, Pont V, Dulac F, Fourmentin M, Lambert D, Sauvage B (2015) Aerosol vertical distribution, optical properties and transport over Corsica (western Mediterranean). Atmos. Chem. Phys. Discuss., 15, 9507-9540, 2015, doi: 10.5194/acpd-15-9507-2015.

Liao H, Seinfeld J (1998) Radiative Forcing by mineral dust aerosols: sensitivity to key variables, J. Geophys. Res., 103, 31637–31645.

Lee YC, Wenig M, Zhang Z (2012) Dust episodes in Hong Kong (South China) and their relationship with the Sharav and Mongolian cyclones and jet stream, Air Qual Atmos Health (2012) 5:413–424, doi: 10.1007/s11869-011-0134-7.

Madonna F, Amodeo A, Boselli A, Cornacchia C, Cuomo V, D'Amico G, Giunta A, Mona L, Pappalardo G (2011) CIAO: the CNR-IMAA advanced observatory for atmospheric research, Atmos. Meas. Tech., 4, 1191-1208, doi:10.5194/amt-4-1191-2011.

Mallet M, Dulac F, Formenti P, Nabat P, Sciare J, Roberts G, Pelon J, Ancellet G, Tanré D, Parol F, Denjean C, Brogniez G, di Sarra A, Alados-Arboledas L, Arndt J, Auriol F, Blarel L, Bourrianne T, Chazette P, Chevaillier S, Claeys M, D' Anna B, Derimian Y, Desboeufs K, Di Iorio T, Doussin JF, Durand P, Féron A, Freney E, Gaimoz C, Goloub P, Gómez-Amo JL, Granados-Muñoz MJ, Grand N, Hamonou E, Jankowiak I, Jeannot M, Léon JF, Maillé M, Mailler S, Meloni D, Menut L, Momboisse G, Nicolas J, Podvin T, Pont V, Rea G, Renard JB, Roblou L, Schepanski K, Schwarzenboeck A, Sellegri K, Sicard M, Solmon F, Somot S, Torres B, Totems J, Triquet S, Verdier N, Verwaerde C, Waquet F, Wenger J, Zapf P (2016) Overview of the Chemistry-Aerosol Mediterranean Experiment/Aerosol Direct Radiative Forcing on the Mediterranean Climate (ChArMEx/ADRIMED) summer 2013 campaign, Atmos. Chem. Phys., 16, 455-504, doi: 10.5194/acp-16-455-2016.

Mamouri RE, Nisantzi A, Ansmann A, Hadjimitsis DG (2016) Extreme dust storm over the eastern Mediterranean in September 2015: Lidar vertical profiling of desert dust at Limassol, Cyprus, Atmos. Chem. Phys. Discuss., doi:10.5194/acp-2016-354.

Marbà N, Jordà G, Agustí S, Girard C, Duarte CM (2015) Footprints of climate change on Mediterranean Sea biota. Front. Mar. Sci. 2:56. doi: 10.3389/fmars.2015.00056.

Martin-Vide J, Lopez-Bustins JA (2006) The western Mediterranean oscillation and rainfall in the Iberian Peninsula. International Journal of Climatology, 26: 1455-1475, doi: 10.1002/joc.1388.

Meloni D, Di Sarra A, DeLuisi J, Di Iorio T, Fiocco G, Junkermann W, Pace G (2003) Tropospheric aerosols in the Mediterranean: 2. Radiative effects through model simulations and measurements, J. Geophys. Res., 108, 4317, doi: 10.1029/2002JD002807.

Meloni D, Di Sarra A, Di Iorio T, Fiocco G (2004) Direct radiative forcing of Saharan dust in 30 the Mediterranean from measurements at Lampedusa Island and MISR space-borne observations, J. Geophys. Res., 109, D08206, doi: 10.1029/2003JD003960.

Meloni D, Di Sarra A, Monteleone F, Pace G, Piacention S, Sferlazzo DM (2008) Seasonal transport patterns of intense dust events at the Mediterranean island of Lampedusa, Atmos. Res., 88, 134–148, doi:10.1016/j.atmosres.2007.10.007.

Mona L, Liu Z, Müller D, Omar A, Papayannis A, Pappalardo G, Sugimoto N, Vaughan M (2012) Lidar measurements for desert dust characterization: an overview, Advances in Meteorology, 2012-article ID: 356265.

Mona L, Papagiannopoulos N, Basart S, Baldasano JM, Binietoglou I, Cornacchia C, Pappalardo G (2014) EARLINET dust observations vs. BSC-DREAM8b modeled profiles: 12-year-long systematic comparison at Potenza, Italy, Atmos. Chem. Phys., 14, 8781-8793, doi:10.5194/acp-14-8781-2014.

Müller D, Heinold B, Tesche M, Tegen I, Althausen D, Arboledas-Arboledas L, Amiridis V, Amodeo A, Ansmann A, Balis D, Comeron A, D'Amico G, Gerasopoulos E, Guerrero-Rascado JL, Freudenthaler V, Giannakaki E, Heese B, Iarlori M, Knippertz P, Mamouri R E, Mona L, Papayannis A, Pappalardo G, Perrone RM, Pisani G, Rizi V, Sicard M, Spinelli N, Tafuro A, Wiegner M (2009) EARLINET Observations of the 14-22-May Long-Range Dust Transport Event During SAMUM 2006: Validation of Results From Dust

Transport Modelling, Tellus B, 61B, 325 – 339, 61B, doi: 10.1111/j. 1600-0889.2008.00400.x.

Müller D, Weinzierl B, Petzold A, Kandler K, Ansmann A, Müller T, Tesche M, Freudenthaler V, Esselborn M, Heese B, Althausen D, Schladitz A, Otto S, Knippertz P (2010) Mineral dust observed with AERONET Sun photometer, Raman lidar and in situ instruments during SAMUM 2006: Shape-independent particle properties, Journal of Geophysical Research, 115, D07202, doi:10.1029/2009JD012520.

Nowottnick EP, Colarco PR, Welton EJ, da Silva A (2015) Use of the CALIOP vertical feature mask for evaluating global aerosol model, Atmos. Meas. Tech., 8, 3647–3669, doi:10.5194/amt-8-3647-2015.

Osada K, Ura S, Kagawa M, Mikami M, Tanaka TY, Matoba S, Aoki K, Shinoda M, Kurosaki Y, Hayashi M, Shimizu A, Uematsu M (2014) Wet and dry deposition of mineral dust particles in Japan: factors related to temporal variation and spatial distribution, Atmos. Chem. Phys., 14, 1107–1121, doi:10.5194/acp-14-1107-2014.

Papayannis A, Mamouri RE, Amiridis V, Kazadzis S, Pérez C, Tsaknakis G, Kokkalis P, Baldasano JM (2009) Systematic lidar observations of Saharan dust layers over Athens, Greece in the frame of EARLINET project (2004-2006), Ann. Geophys., 27, 3611–3620.

Pappalardo G, Amodeo A, Apituley A, Comeron A, Freudenthaler V, Linné H, Ansmann A, Bösenberg J, D'Amico G, Mattis I, Mona L, Wandinger U, Amiridis V, Alados-Arboledas L, Nicolae D, Wiegner M (2014) EARLINET: towards an advanced sustainable European aerosol lidar network, Atmos. Meas. Tech., 7, 2389–2409.

Pelon J, Flamant C, Chazette P, Leon JF, Tanre D, Sicard M, Satheesh S K (2002) Characterization of aerosol spatial distribution and optical properties over the Indian Ocean from airborne LIDAR and radiometry during INDOEX'99, J. Geophys. Res.-Atmos., 107, 8029, doi: 10.1029/2001JD000402.

Pérez C, Nickovic S, Baldasano JM, Sicard M, Rocadenbosch F, Cachorro VE (2006a) A long Saharan dust event over the western Mediterranean: Lidar, Sun photometer observations, and regional dust modeling, J. Geophys. Res., 111, D15214, doi: 10.1029/2005JD006579.

Pérez C, Nickovic S, Pejanovic G, Baldasano JM, Özsoy E (2006b) Interactive dust-radiation modeling: A step to improve weather forecasts, J. Geophys. Res., 111, D16206, doi:10.1029/2005JD006717.

Perrone MR, De Tomasi F, Gobbi GP (2014b) Vertically resolved aerosol properties by multi-wavelength lidar measurements, Atmos. Chem. Phys., 14, 1185–1204, doi: 10.5194/acp-14-1185-2014.

Prospero JM, Ginoux P, Torres O, Nicholson SE, Gill TE (2002),Environmental characterization of global sources of atmospheric soil dust identified with the nimbus 7 total ozone mapping spectrometer (TOMS) absorbing aerosol product, Rev. Geophys.,40(1), 1002, doi:10.1029/2000RG000095.

Ricchiazzi P, Yang S, Gautier C, Sowle D (1998) SBDART: A Research and Teaching Software Tool for Plane-Parallel Radiative Transfer in the Earth's Atmosphere, B. Am. Meteor. Soc., 79, 2101–2114, doi:10.1175/1520-0477(1998).

Romano S, Burlizzi P, Perrone MR (2016) Experimental determination of short- and long-wave dust radiative effects in the Central Mediterranean and comparison with model results. Atmos. Res. 171, 5-20, doi: 10.1016/j.atmosres.2015.11.019.

Russell PB, Bergstrom RW, Shinozuka Y, Clarke AD, De-Carlo PF, Jimenez JL, Livingston JM, Redemann J, Dubovik O, Strawa A (2010) Absorption Angstrom Exponent in AERONET and related data as an indicator of aerosol composition, Atmos. Chem. Phys., 10, 1155–1169, doi:10.5194/acp-10-1155-2010.

Sanchez-Gomez E, Somot S, Mariotti A (2009) Future changes in the Mediterranean water budget projected by an ensemble of regional climate models, Geophys. Res. Lett., 36, 30 L21401, doi:10.1029/2009GL040120.

Seinfeld JH, Pandis SN (1998) Atmospheric Chemistry and Physics: From Air Pollution to Climate Change. J. Wiley &Sons, INC.

Sicard M, Rocadenbosch F, Reba MNM, Comerón A, Tomás S, García-Vizacíno D, Batet O, Barrios R, Kumar D, Baldasano JM (2011) Seasonal variability of aerosol optical properties observed by means of a Raman lidar at an EARLINET site over Northeastern Spain, Atmos. Chem. Phys., 11, 175-190, doi:10.5194/acp-11-175-2011.

Sicard M, Mallet M, García-Vizcaíno D, Comerón A, Rocadenbosch F, Dubuisson P, Muñoz-Porcar C (2012) Intense dust and extremelly fresh biomass burning in Barcelona, Spain: characterization of their optical properties and estimation of their radiative forcing, Environ. Res. Lett., 7, 034016, doi:10.1088/1748-9326/7/3/034016.

Sicard M, Bertolín S, Mallet M, Dubuisson P, Comerón A (2014) Estimation of mineral dust long-wave radiative forcing: sensitivity study to particle properties and application to real cases in the region of Barcelona, Atmos. Chem. Phys., 14, 9213–9231, doi:10.5194/acp-14-9213-2014.

Sicard M, Barragan R, Muñoz-Porcar C, Comerón A, Mallet M, Dulac F, Pelon J, Alados-Arboledas L, Amodeo A, Boselli A, Bravo-Aranda JA, D'Amico G, Granados-Muñoz MJ, Leto G, Guerrero-Rascado JL, Madonna F, Mona L, Pappalardo G, Perrone MR, Burlizzi P, Rocadenbosch F, Rodríguez-Gómez A, Scollo S, Spinelli N¸ Titos G, Wang X, Zanmar Sanchez R (2016a) Contribution of EARLINET/ACTRIS to the summer 2013 Special Observing Period of the ChArMEx project: monitoring of a Saharan dust event over the western and central Mediterranean, International Journal of Remote Sensing, in press.

Sicard M, Barragan R, Dulac F, Alados-Arboledas L, Mallet M (2016b) Aerosol optical, microphysical and radiative properties at three regional background insular sites in the western Mediterranean Basin, Atmos. Chem. Phys. Discuss., doi:10.5194/acp-2015-823.

Stein AF, Draxler RR, Rolph GD, Stunder BJB, Cohen MD (2015) NOAA´s HYSPLIT Atmospheric transport and dispersion modelling system, American Meteorological Society, doi: 10.1175/BAMS-D-14-00110.1.

Tafuro AM, Barnaba F, De Tomasi F, Perrone MR, Gobbi GP (2006) Saharan dust particle properties over the central Mediterranean, Atmospheric Research, 81, 67-93, doi: 10.1016/j.atmosres.2005.11.008.

Thieuleux F, Moulin C, Bréon FM, Maignan F, Poitou J, Tanré D (2005) Remote Sensing of Aerosols over the oceans using MSG/SEVIRI Imagery, Ann. Geophys., 23, 3561-3568, doi:10.5194/angeo-23-3561-2005.

Valenzuela A, Olmo FJ, Lyamani H, Antón M, Titos G, Cazorla A, Alados-Arboledas L (2015) Aerosol scattering and absorption Angström exponents as indicators of dust and dust-free days over Granada (Spain). Atmos Res 154:1–13.

Valenzuela A, Olmo FJ, Lyamani H, Antón M, Quirantes A, Alados-Arboledas L (2012) Aerosol radiative forcing during African desert dust events (2005–2010) over Southeastern Spain, Atmos. Chem. Phys. 12, 10331-10351.

Tables and figures

Station	Location (◦ N, ◦ E)	Altitude (m.a.m.s.l.)	Lidar channels	λ ß (nm)	Spatial resolution (m)	Reference	AERONET Sun-photometer
Granada	37.16, −3.61	680	3ß+2α+1δ	532, 355, 1064	7.5	Guerrero-Rascado et al. (2008)	Y
Barcelona	41.39, 2.17	115	3ß+2α+WV	532, 355, 1064	3.75/2.3	Sicard et al. (2011)	Y
Cap d'en Font	39.49, 4.12	10	1ß+1α+1δ	355	5.25	Chazette et al. (2016)	Y
Ersa	48.42, 2.10	20	1ß+1α+1δ	355	15	León et al. (2015)	Y
Potenza	40.60, 15.72	760	3ß+2α+1δ	532, 355, 1064	60	Madonna et al. (2011)	Y
Naples	40.50, 14.10	118	2ß+1δ	532, 355	60	Armenante et al. (2009)	N
Lecce	40.30, 18.10	30	3ß+2α+1δ+WV	532, 355, 1064	45	Perrone et al. (2014b)	Y
Serra la Nave	37.68, 14.98	1735	1ß+1δ	355	60	Mallet et al. (2016)	N

Table 1. Characteristics of the lidar systems and the presence of co-located AERONET Sun-photometers. ß is for the backscatter channels, α for the extinction channels and δ for the depolarization channels. WV means that a water vapor channel is available in the lidar system.

Station	AOD_{440}			$AE_{440-870}$			Coarse fraction (440)
	Max (date)	Min (date)	Mean	Max (date)	Min (date)	Mean	
Granada	0.268 (16 june 16:22)	0.185 (15 June 17:47)	0.23	0.66 (15 June 16:53)	0.423 (16 June 16:22)	0.43	0,51
Barcelona							
Cap d'en Font	0.376 (16 June 17:19)	0.154 (16 June 07:07)	0.25	1,032 (16 June 06:11)	0.416 (16 June 15:52)	0.46	0,39
Ersa	0.359 (19 June 17:33)	0.062 (18 June 17:32)	0.21	1.754 (19 June 05:47)	0.857 (19 June 15:33)	1.26	0,25
Potenza	0.160 (21 June 17:03)	0.073 (23 June 15:08)	0.145	1.559 (23 June 17:03)	0.551 (21 June 16:35)	0.86	0,28
Lecce	0.331 (23 June 04:48)	0.12 (21 June 14:57)	0.234	1.777 (21 June 04:48)	0.715 (23 June 04:48)	1.07	0,25

Table 2. AERONET level 2.0 AOD, AE maximum, minimum and mean values and mean value of the Coarse Fraction calculated for the days with aerosol presence at each station, 15-16-17 at Granada, 16-17 at Cap d'en Font, 17-18-19-20 at Ersa, 21-22-23 at Potenza and 21-22-23 at Lecce.

Station	Temporal Coarse fraction									
	15 June	16 June	17 June	18 June	19 June	20 June	21 June	22 June	23 June	24 June
Granada	0,48	0,56	0,53							
Barcelona										
Cap d'en Font		0,44	0,53							
Ersa			0,25	0,26	0,26	0,25				
Potenza							0,50	0,40	0,19	
Lecce							0,12	0,34	0,41	

Table 3. Spatio-temporal evolution of the AERONET level 2.0 Coarse mode fraction.

Station	Bottom height (m)	Top height (m)	Center of mass (m)	Thickness (m)	AOD (Dust)			AE (Dust)		
					532	355	1064	532_1064	532_355	355_1064
Granada	1719	5296	3368	3577	0.26	0.28	0.24	0.06	0.13	0.0861
Barcelona	911	6584	3929	5672	0.37		0.21	0.80		
Cap d'en Font	201	5787	3319	5585		0.37				
Ersa	1360	4948	1778	3587		0.20				
Potenza	1630	5530	2350	3900	0.10	0.13	0.09	0.09	0.50	0.25
Naples	1468	7708	3388	6240	0.13	0.16			0.65	
Lecce	809	6790	2743	5981	0.22	0.23	0.21	0.06	1.72	0.67
Serra la Nave	4010	7910	5330	3900		0.12				

Table 4. Instantaneous height values at the eight stations at the peak moment of the event in each station. The heights represent the bottom and top height of the mineral dust layer. The thickness has been calculated by subtracting the bottom height from the top height. The AOD (dust) are the values of the optical depth retrieved from lidar measurements of the mineral dust layer, not the complete atmospheric column. The backscatter AE values are retrieved from lidar measurements only for the mineral dust layers.

Parameters		Shortwave GAME	Longwave GAME
Spectral range		0.3 – 4 μm	4 – 37 μm
Number of sub-bands		18	40
Atmospheric parameters	Atmospheric profile	Radiosoundings + US Stand. Atmos.	Radiosoundings + US Stand. Atmos.
	H_2O	Radiosoundings	Radiosoundings
	O_3	US Stand. Atmos.	US Stand. Atmos.
	Absorption coefficients of main gases	HITRAN	HITRAN
	Surface albedo	from ground-based measurements	-
	LW emissivity	-	from CERES
Meteo parameters	At the surface	Measured at the meteorological station	
	< 20 km	Radiosoundings	
	> 20 km	US Standard Atmosphere	
Aerosols	AOD	Lidar extinction coefficient	Mie calculation
	Single Scattering Albedo	AERONET	Mie calculation
	Asymmetry factor	AERONET	Mie calculation
	Aerosol vertical distribution	Lidar	Lidar
	Size distribution	-	AERONET
	Fine and coarse mode radius	-	AERONET
	Fine and coarse mode concentration	-	AERONET
	Refractive index	-	Krekov (1993)

Table 5. Input parameters for the Global Atmospheric Model and data sources in the SW and LW spectral ranges.

Station	day	SZA (°)	AOD_{lidar}	SSA	BOA SW-DRF (Wm^{-2})	TOA SW-DRF (Wm^{-2})	BOA LW-DRF (Wm^{-2})	TOA LW-DRF (Wm^{-2})	BOA SW-AER (Wm^{-2})	TOA SW-AER (Wm^{-2})
Granada	16	55	0.17	0.87	-16.9	+1.3	+5.8	+3.7	-38.3	-15.3
	16	67	0.26	0.87	-36.9	+5.8	+6.3	+7.0	-42.6	-11.8
	17	32	0.06	0.83	-42.3	+0.7	+0.3	+0.2	-39	-8.2
									(Cap d'en Font)	(Cap d'en Font)
									(Cap d'en Font)	(Cap d'en Font)
									-29.9 (Cap d'en Font)	-14.4 (Cap d'en Font)
Cap d'en Font	16	27	0.34	0.91	-45.3	-34.5	+10.8	+7.2	-17.5	-12.7
	17	27	0.37	0.91	-44.9	-29.9	+17.7	+8.5	-28.4	-19
	18	85	0.27	0.96	-25.3	-6.8	+1.6	+4.6	-18.1	-9.4
	19	28	0.23	0.96	-18.3	-9.2	+9.8	+8.9	-16.9	-9.6
	20	28	0.12	0.98	-3.5	-2.2	+1.9	+0.5	-14.7	-8.5
									-23.6 (Potenza)	-12.9 (Potenza)
									-25.6 (Potenza)	-13.1 (Potenza)
									-23.4 (Potenza)	-10.11 (Potenza)
Lecce	20	30	0.13	0.94	-15	-5.6	+1.9	+1.6	-20.7	-9.7
	21	25	0.12	0.85	-12	+3.2	+1.5	+1.3	-19.7	-4.7
	22	26	0.22	0.89	-37	+4.3	+3.8	+2.4	-36.9	-14.8
	24	18	0.14	0.99	-7	-2.9	+1.3	+0.9	-14.4	-6

Table 6. Instantaneous short-wave and long-wave radiative forcing at the bottom of the atmosphere and at the top of the atmosphere simulated by the Global Atmospheric Model for the 12 selected cases of June 2013 and retrieved from AERONET measurements. SZA represents the solar zenith angle, AOD and SSA indicate the aerosol optical depth (in the mineral dust layer) and the single scattering albedo (from AERONET Sun-photometer observations) at 440 nm, respectively The negative

values of the radiative forcing correspond to a cooling effect while the positive values correspond to a heating effect of the aerosols.

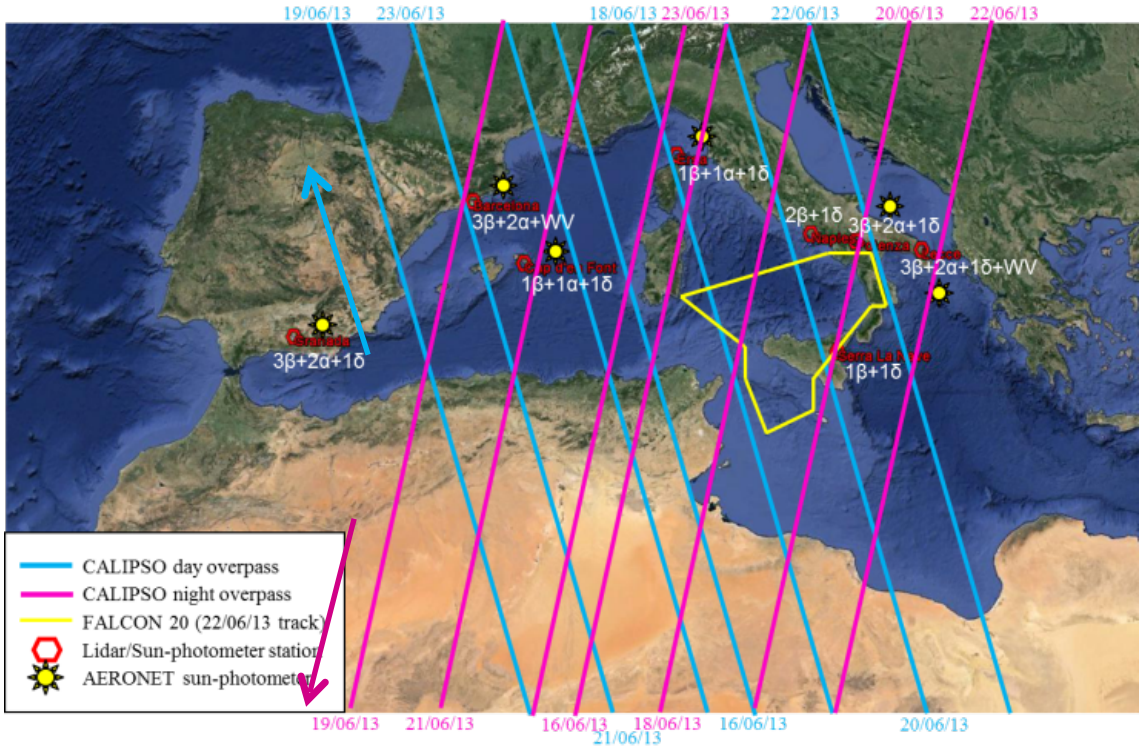

Figure 1. Map of the sites. in red the lidar stations and a yellow sun for the AERONET Sun-photometers Red hexagons represent the sites. The blue lines represent the diurnal CALIPSO overpasses. The yellow line represents the FALCON 20 flight (22/06/13). The blue arrow indicates the direction (ascending, from South to North) of the daytime overpasses, and the pink arrow indicates the direction (descending, from North to south) of the nightly overpasses.

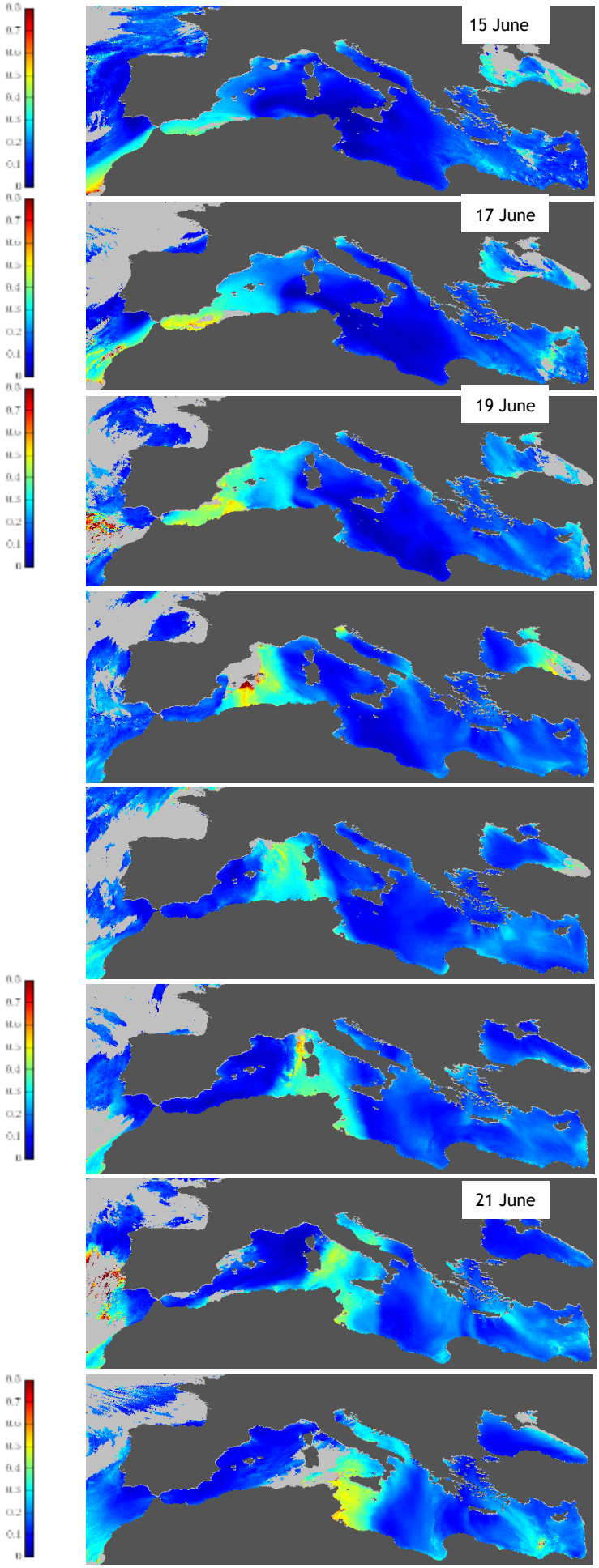
15 June
16 June
17 June
18 June
19 June
20 June
21 June
22 June

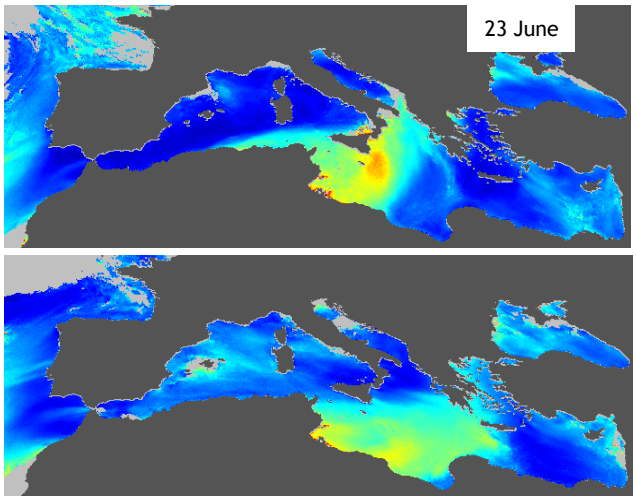

Figure 2. Color map of the aerosol optical depth (at 550 nm) daily mean values over the Mediterranean Sea from the MSG-SEVIRI instrument - ICARE Thematic Center (www.icare.univ.lille1.fr), from 16 to 24 June 2013.

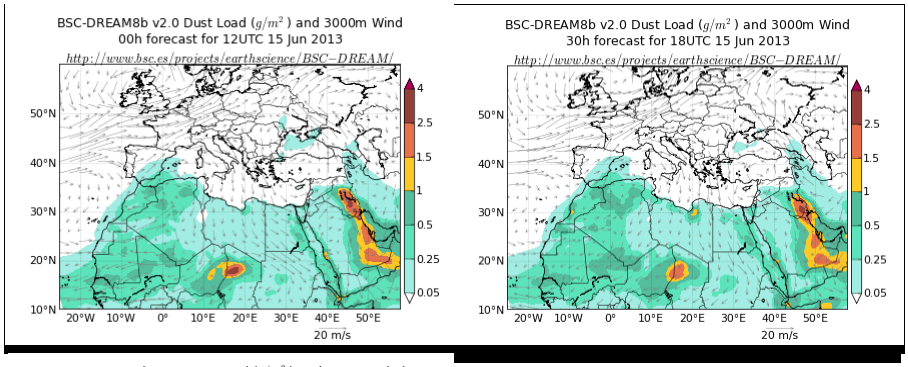
BSC-DREAM8b v2.0 Dust Load (g/m^2) and 3000m Wind
00h forecast for 12UTC 15 Jun 2013
http://www.bsc.es/projects/earthscience/BSC-DREAM/
BSC-DREAM8b v2.0 Dust Load (g/m^2) and 3000m Wind
30h forecast for 18UTC 15 Jun 2013
http://www.bsc.es/projects/earthscience/BSC-DREAM/

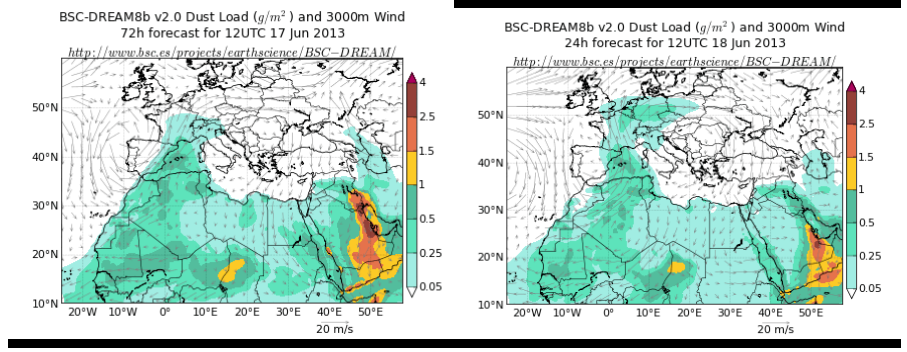
BSC-DREAM8b v2.0 Dust Load (g/m^2) and 3000m Wind
72h forecast for 12UTC 17 Jun 2013
http://www.bsc.es/projects/earthscience/BSC-DREAM/
BSC-DREAM8b v2.0 Dust Load (g/m^2) and 3000m Wind
24h forecast for 12UTC 18 Jun 2013
http://www.bsc.es/projects/earthscience/BSC-DREAM/

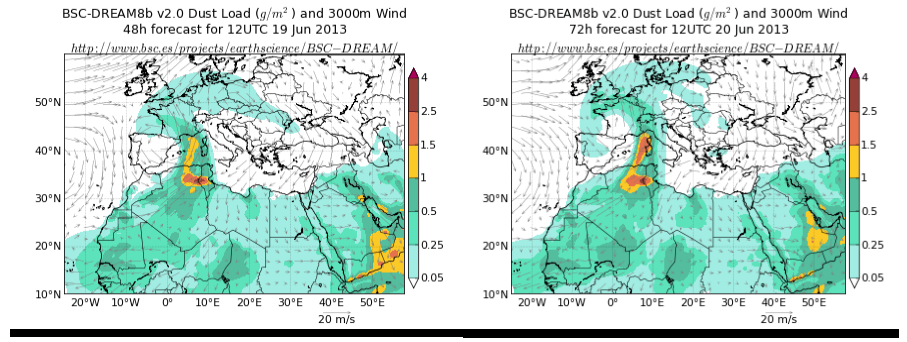
BSC-DREAM8b v2.0 Dust Load (g/m^2) and 3000m Wind
48h forecast for 12UTC 19 Jun 2013
http://www.bsc.es/projects/earthscience/BSC-DREAM/
BSC-DREAM8b v2.0 Dust Load (g/m^2) and 3000m Wind
72h forecast for 12UTC 20 Jun 2013
http://www.bsc.es/projects/earthscience/BSC-DREAM/

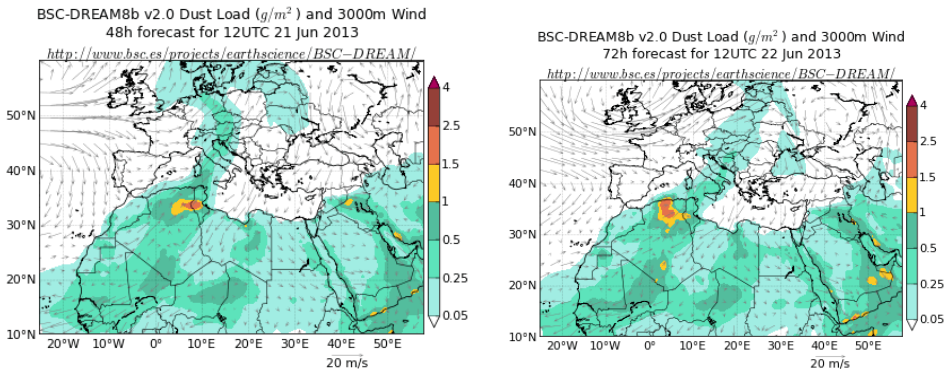
BSC-DREAM8b v2.0 Dust Load (g/m^2) and 3000m Wind
48h forecast for 12UTC 21 Jun 2013
http://www.bsc.es/projects/earthscience/BSC-DREAM/
BSC-DREAM8b v2.0 Dust Load (g/m^2) and 3000m Wind
72h forecast for 12UTC 22 Jun 2013
http://www.bsc.es/projects/earthscience/BSC-DREAM/

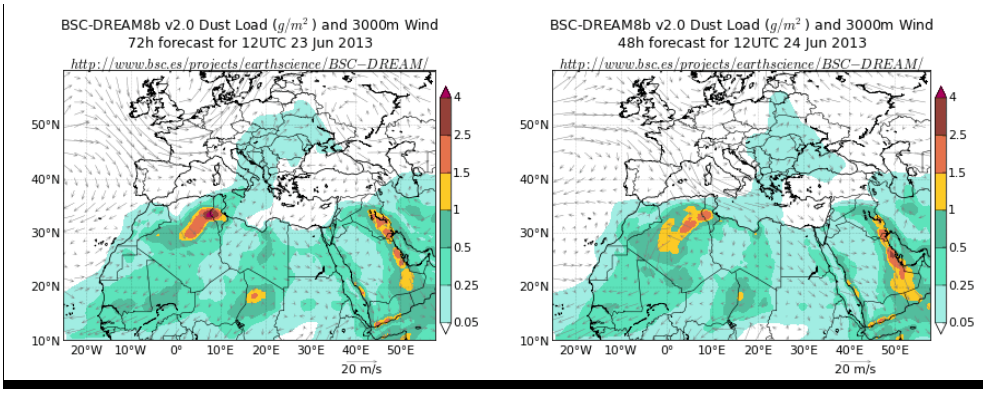
BSC-DREAM8b v2.0 Dust Load (g/m^2) and 3000m Wind
72h forecast for 12UTC 23 Jun 2013
http://www.bsc.es/projects/earthscience/BSC-DREAM/
BSC-DREAM8b v2.0 Dust Load (g/m^2) and 3000m Wind
48h forecast for 12UTC 24 Jun 2013
http://www.bsc.es/projects/earthscience/BSC-DREAM/

Figure 3. BSC-DREAM8b model images, from 15 to 24 june. The colored areas correspond to the presence of aerosol in the atmosphere.

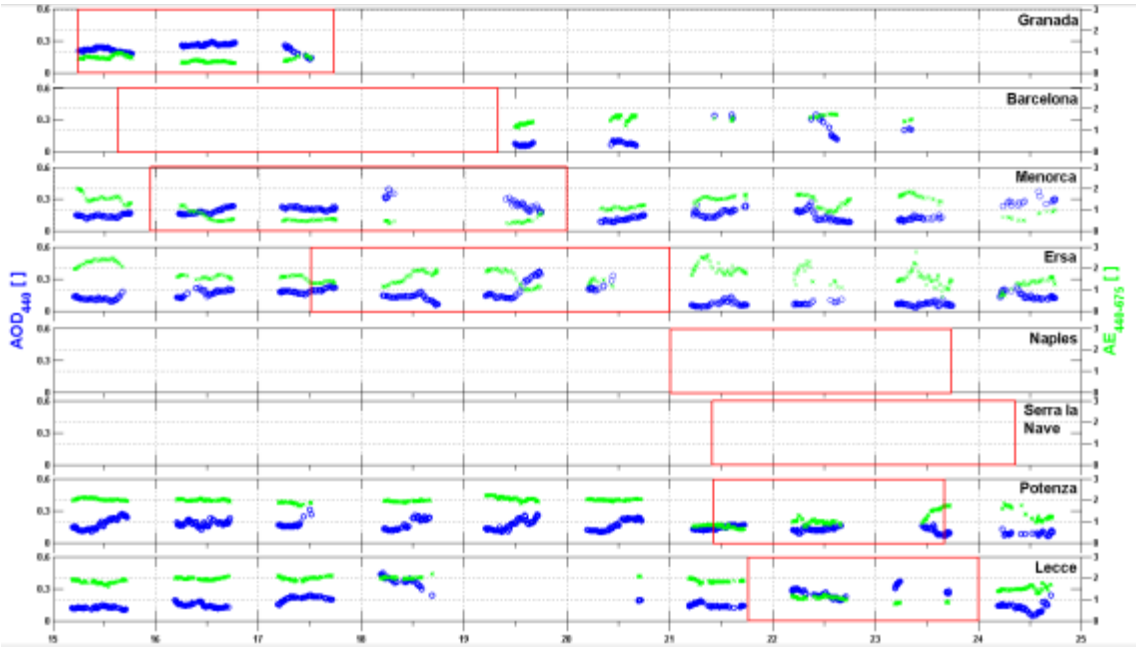

(a)

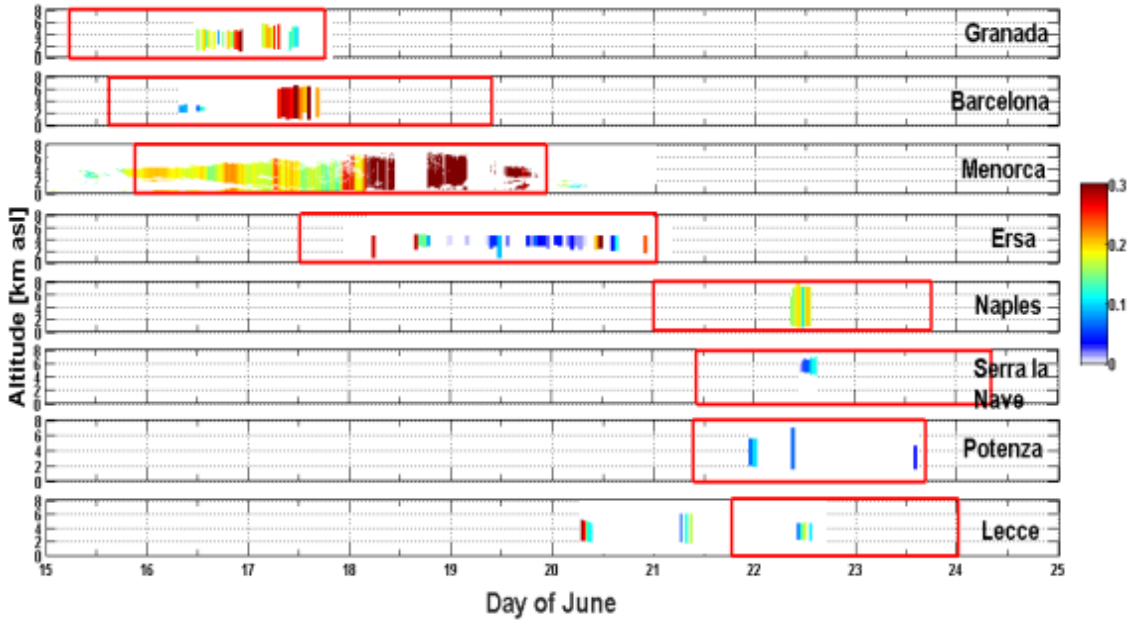

(b)

Figure 4. a) Temporal evolution of the AERONET AOD (blue circles) and and AE (green crosses) in the eight stations of the study, the red boxes show the presence of mineral dust following the criteria explained in the Section 3.1. b) Temporal evolution of the mineral dust plume optical depth retrieved from lidar profiles in the eight stations.

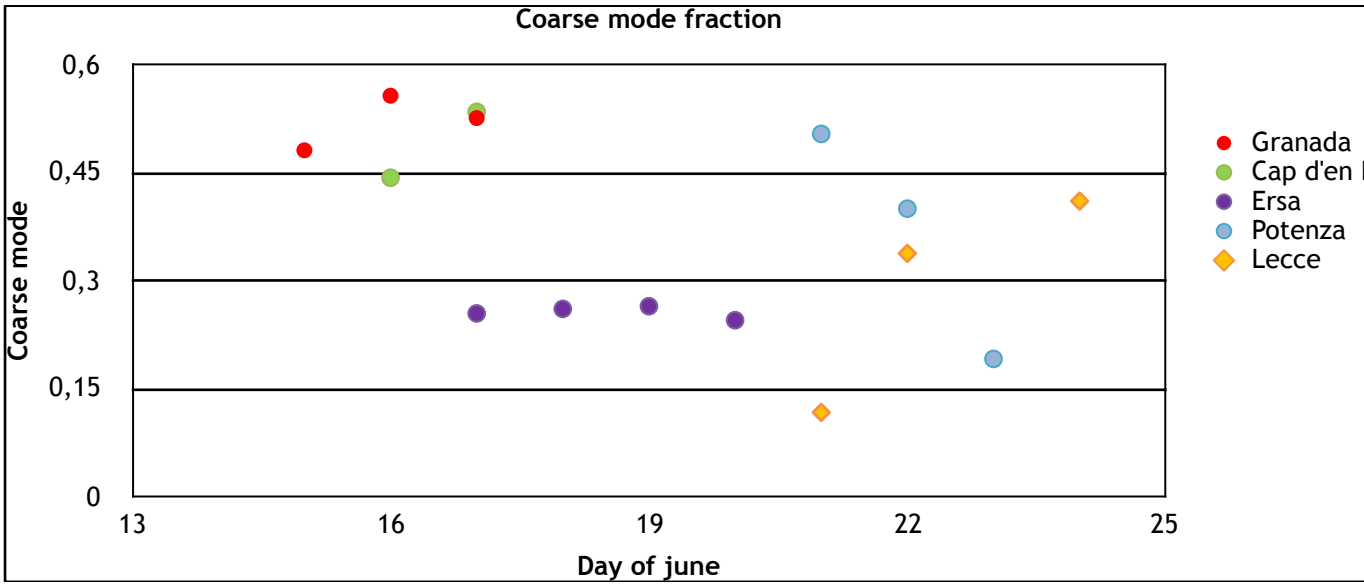

(a)

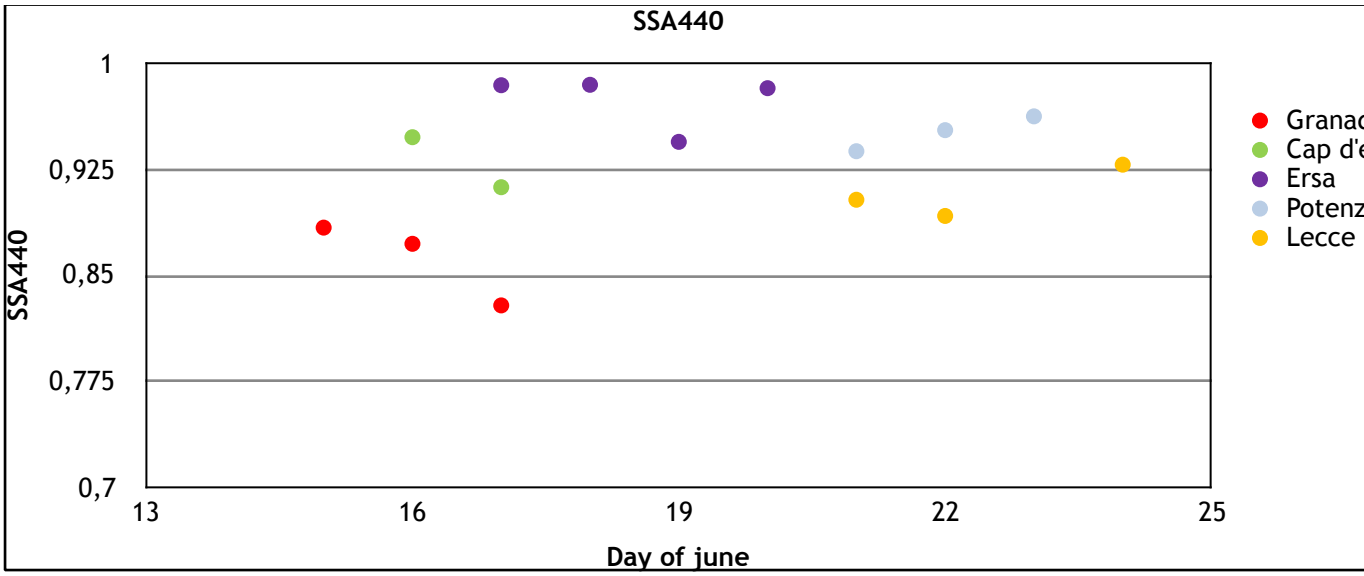

(b)

Figure 5. Temporal evolution of the AERONET level 2.0 data (a) Coarse mode fraction and (b) SSA in Granada (red), Cap d'en Font (green), Ersa (purple), Potenza (grey) and Lecce (yellow).

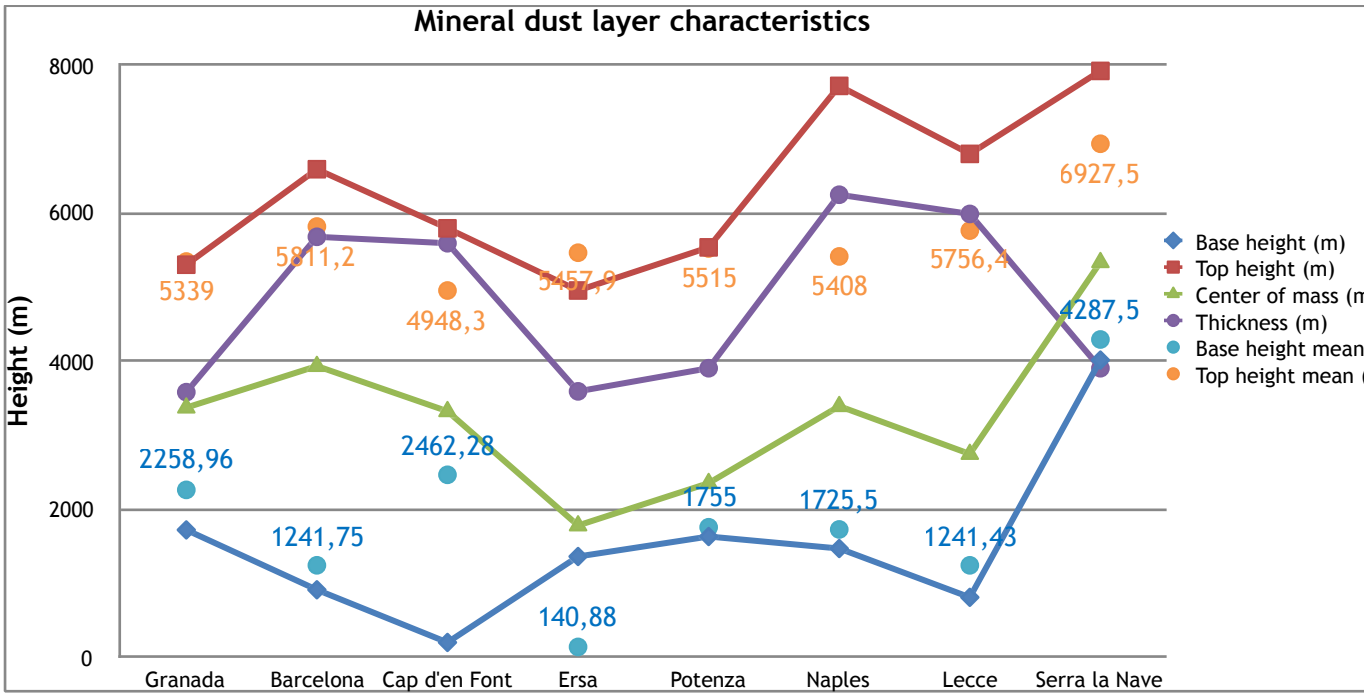

Figure 6. Spatial evolution of the characteristics of the mineral dust layer, during the peak moments (lines) and the mean of the event (dots and stars), retrieved by lidar measurements. In blue the base of the mineral dust layer, in red the top height of the layer and in purple the thickness (top height minus bottom height) of the mineral dust layer. In green is represented the center of mass of the layer.

a)

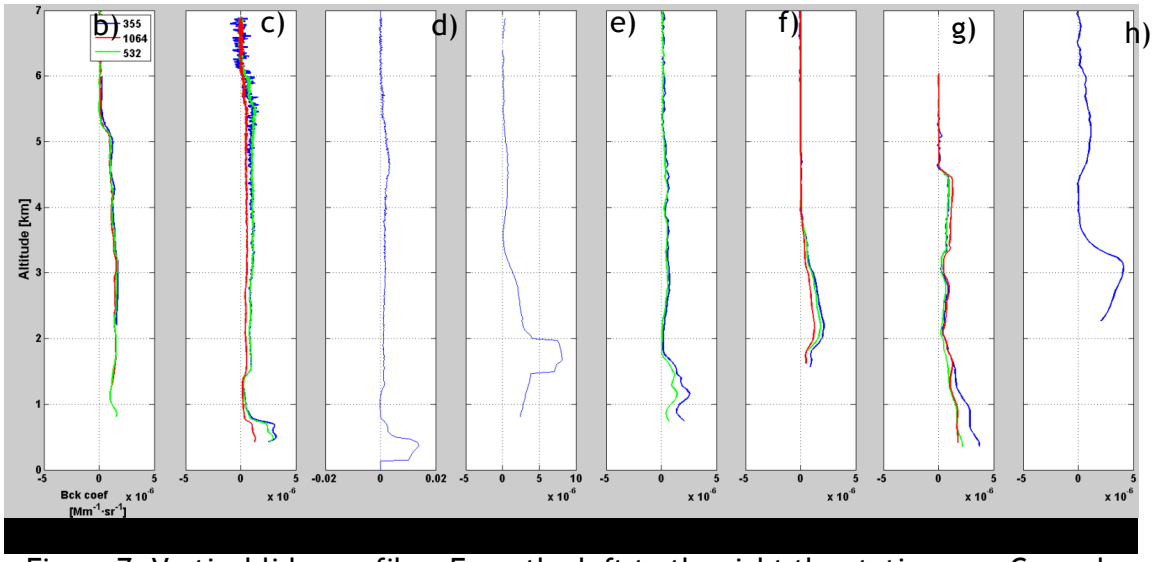

Figure 7. Vertical lidar profiles. From the left to the right the stations are Granada (a), Barcelona (b), Cap d'en Font (c), Ersa (d), Naples (e), Potenza (f), Lecce (g) and Serra la Nave (h). The date of the measurements are 17 June at 01 UTC, 17 June at 08 UTC, 18 June at 12 UTC, 20 June at 15 UTC, 22 June at 10:46 UTC, 21 June at 23:40, 22 June at 11:18 and 22 June at 12:56 for Granada, Barcelona, Cap d'en Font, Ersa, Naples, Potenza, Lecce and Serra la Nave respectively. The green curves represent the backscatter profile at 532 nm, the blue and red lines represent the backscatter profile at 355 and 1064 nm respectively.

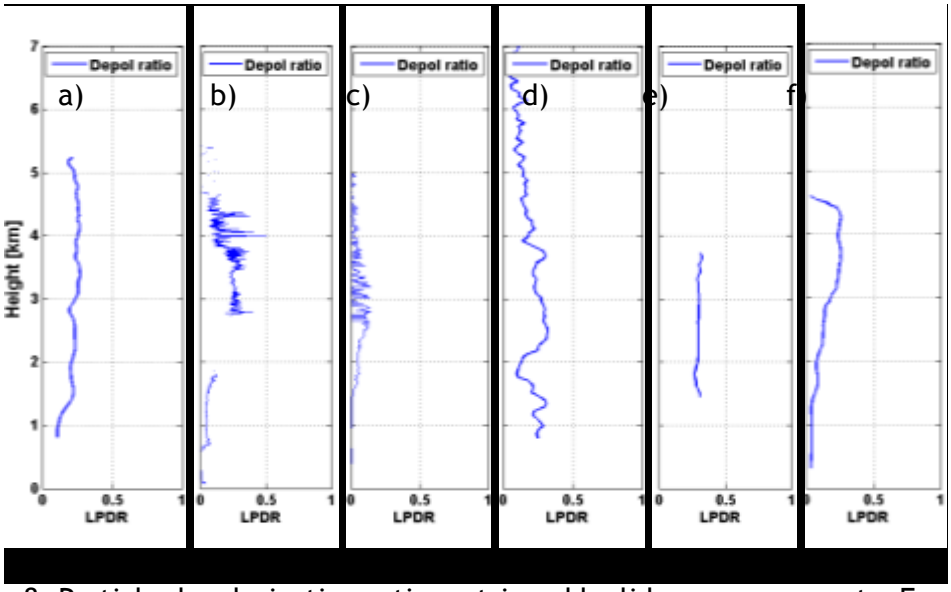

Figure 8. Particle depolarization ratios retrieved by lidar measurements. From the left to the right the stations are Granada at 532 nm (a), Cap d'en Font at 355 nm (b), Ersa at 355 nm (c), Naples at 532 nm (d), Potenza at 532 nm (e), Lecce at 355 nm (f). The date of the measurements are 17 June at 01 UTC, 18 June at 12 UTC, 20 June at 15 UTC, 22 June at 10:46 UTC, 21 June at 23:40 and 22 June at 11:18 for Granada, Cap d'en Font, Ersa, Naples, Potenza and Lecce respectively. The bottom and top heights are 2236 and 5994 m in Granada, 201 and 5787 m in Cap d'en Font, 1360 and 4848 m in Ersa, 1768 and 7468 m in Naples, 1630 and 5530 m in Potenza and 1484 and 5081 m in Lecce.

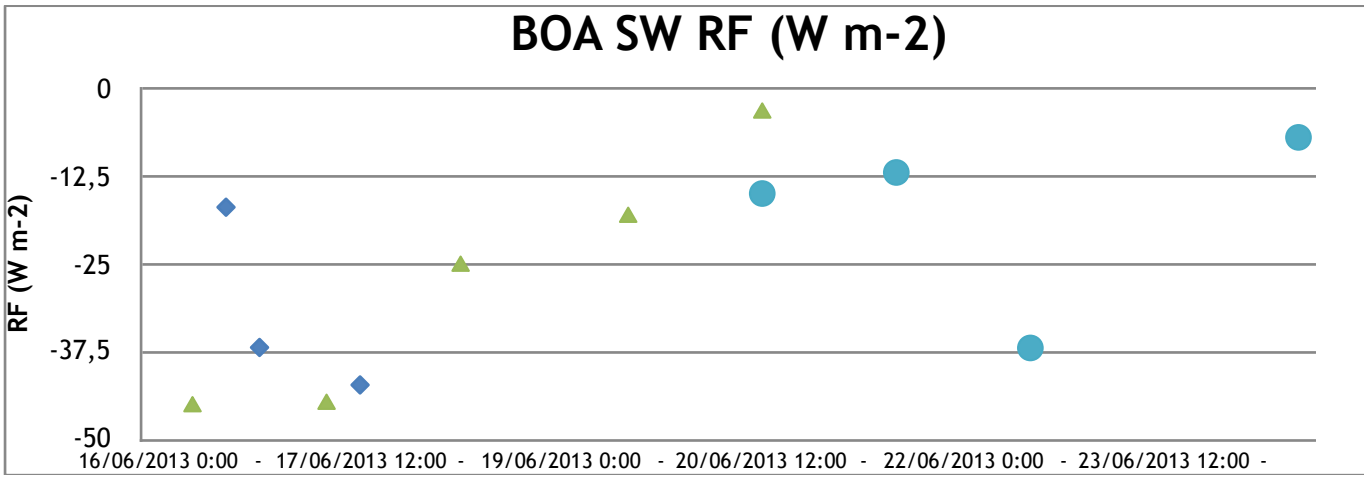

(a)

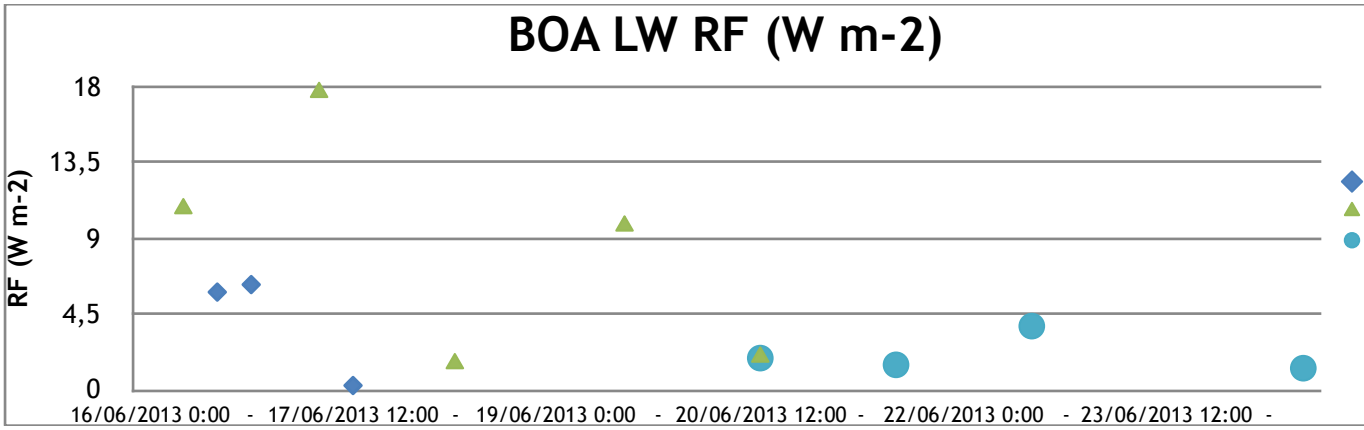

(b)

Figure 9. Temporal evolution of the short-wave (a) and long-wave (b) radiative forcing (W m^{-2}) at the Bottom of the Atmosphere simulated by GAME in Granada (blue diamonds), Cap d'en Font (green triangles) and Lecce (blue lines).

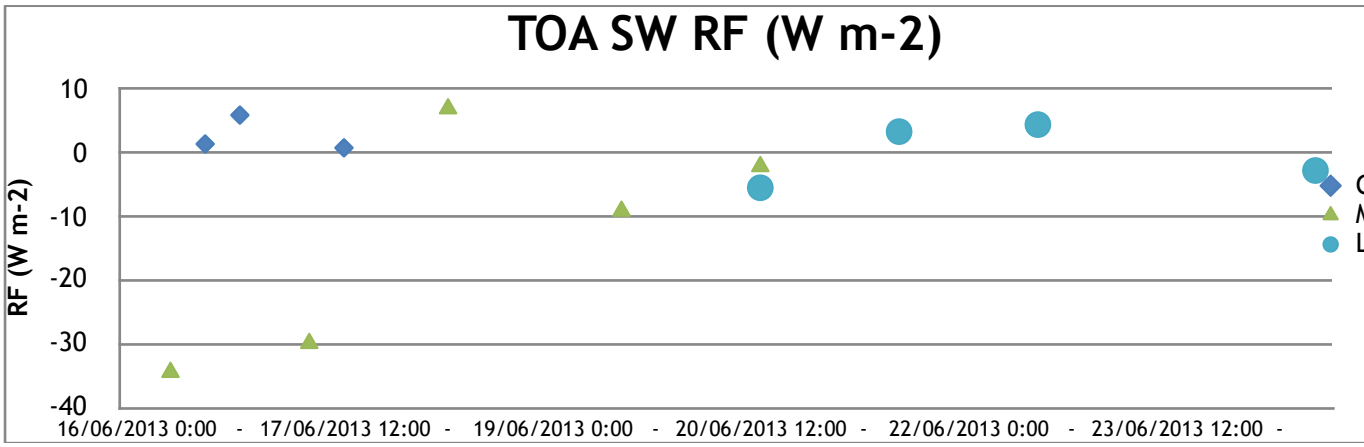

(a)

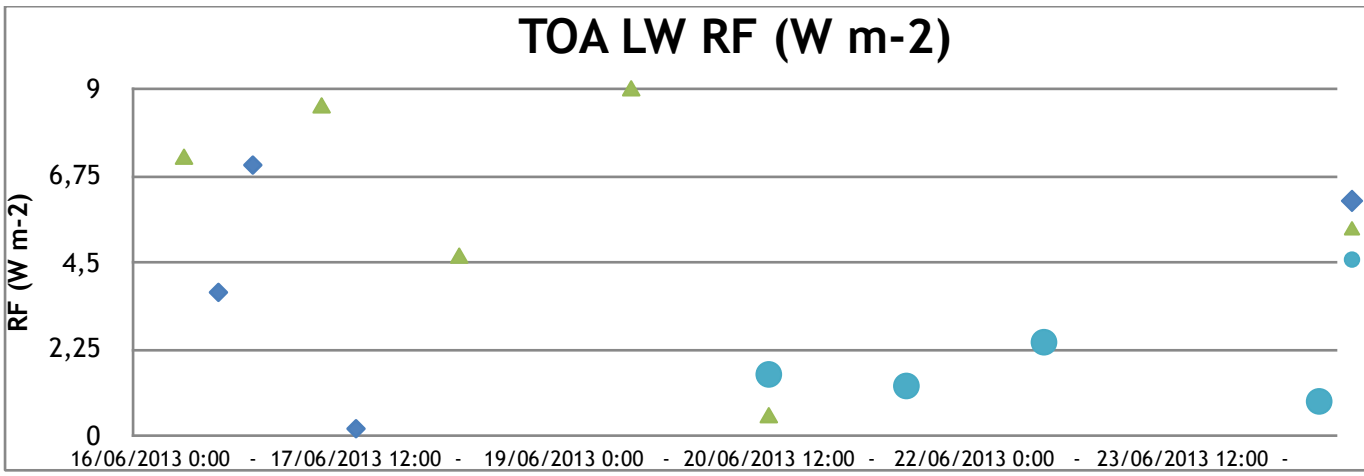

(b)

Figure 10. Temporal evolution of the short-wave (a) and long-wave (b) radiative forcing (W m^{-2}) at the Top of the Atmosphere simulated by GAME in Granada (blue diamonds), Cap d'en Font (green triangles) and Lecce (blue lines).

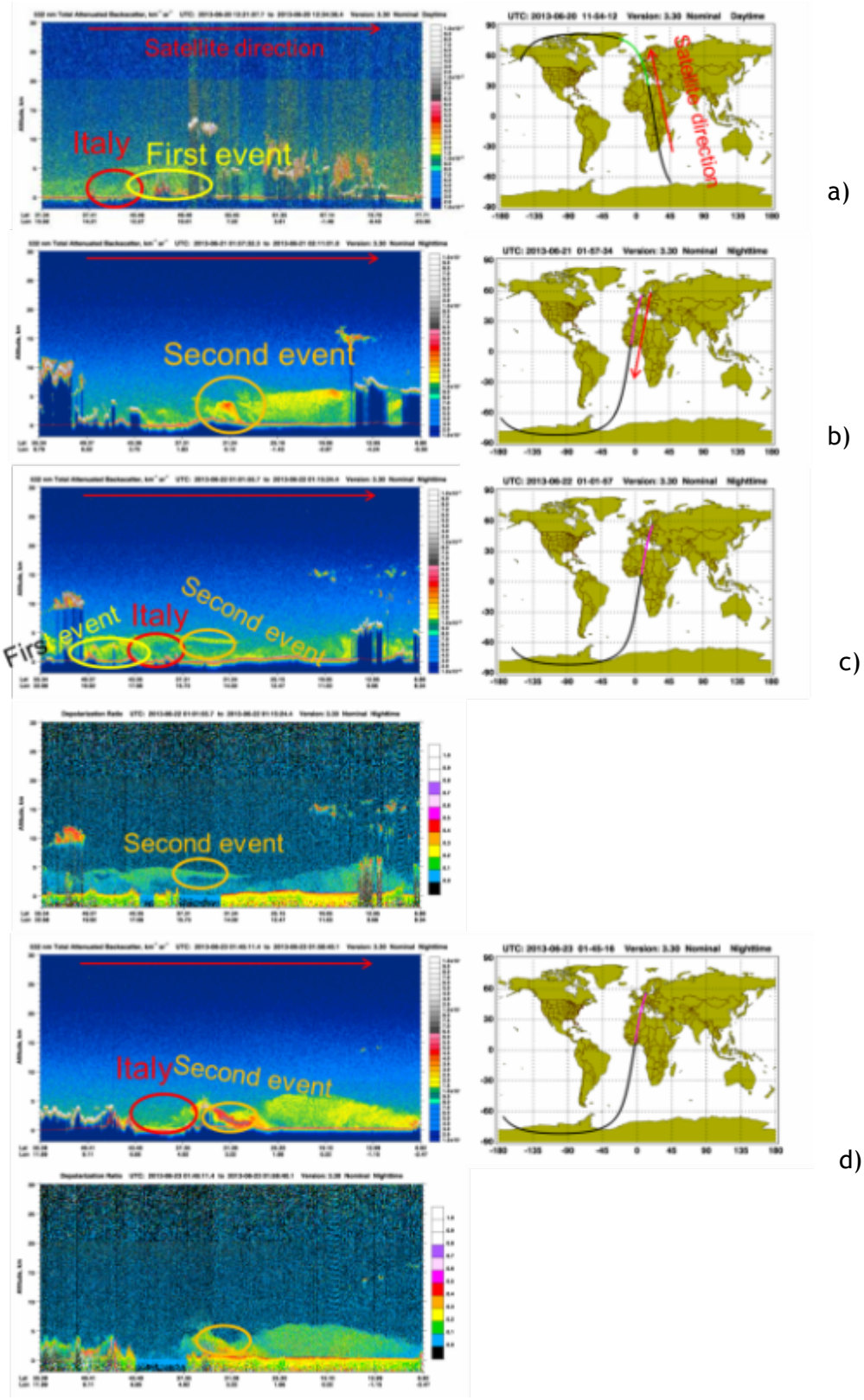

Figure 11. Spatio-temporal evolution of the dust plume monitored by CALIPSO overpasses. In red Italy, in yellow the first Saharan dust event and in orange the second Saharan dust event. a) Attenuated backscatter figure of the day time overpass of the 20 June. b) Attenuated backscatter figure of the night time overpass of the 21 June. c) Attenuated backscatter and lidar particle depolarization ratio figures of the night time overpass of the 22 June. d) Attenuated backscatter and lidar particle depolarization ratio figures of the night time overpass of the 23 June.

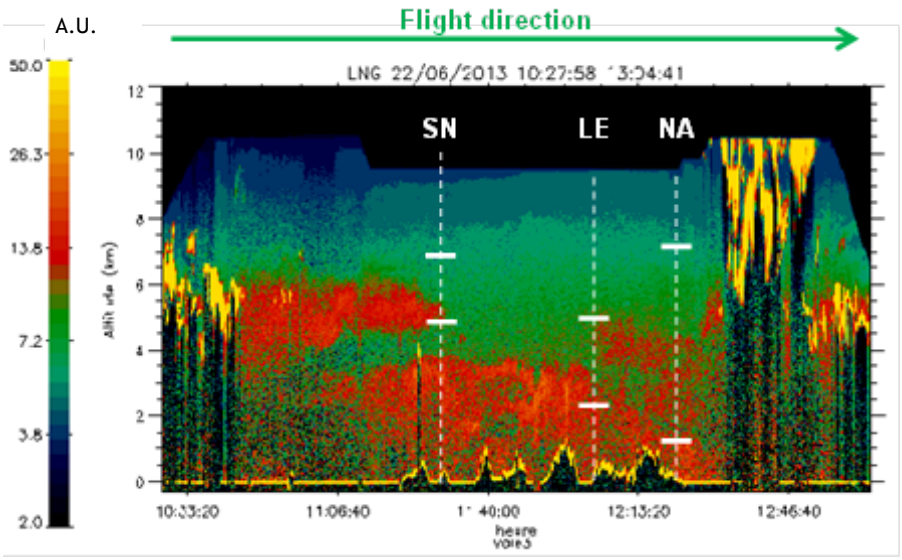

Figure 12. Attenuated backscatter figure of the French Falcon 20 flight on 22 June. The green arrow represents the flight direction. The dash lines are the location of three Italian stations (SN for Serra la Nave, LE for Lecce and NA for Naples), the white lines represents the bottom and top heights of the mineral dust layers detected by the lidars. The red areas correspond to the presence of aerosol.

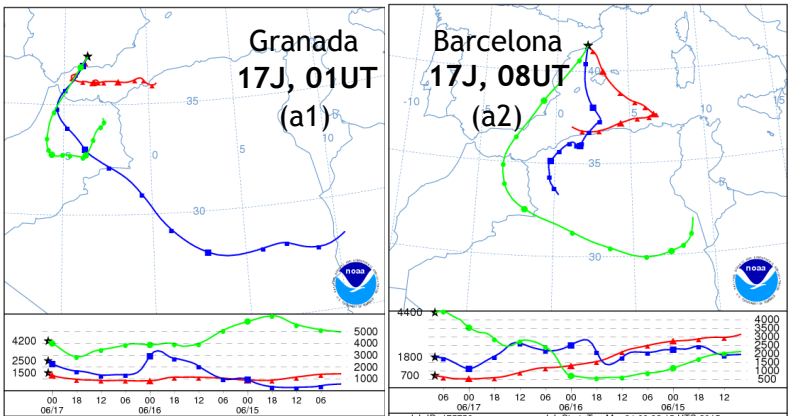

Cap d'en
16J, 12UT
(b1)

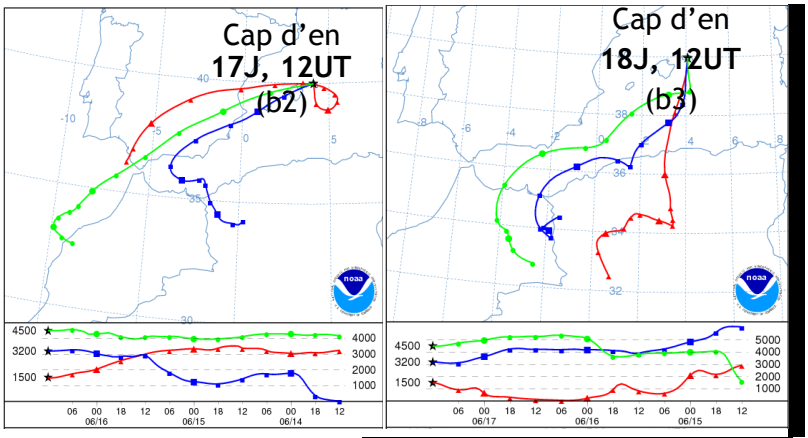

Cap d'en
19J, 12UT
(b4)

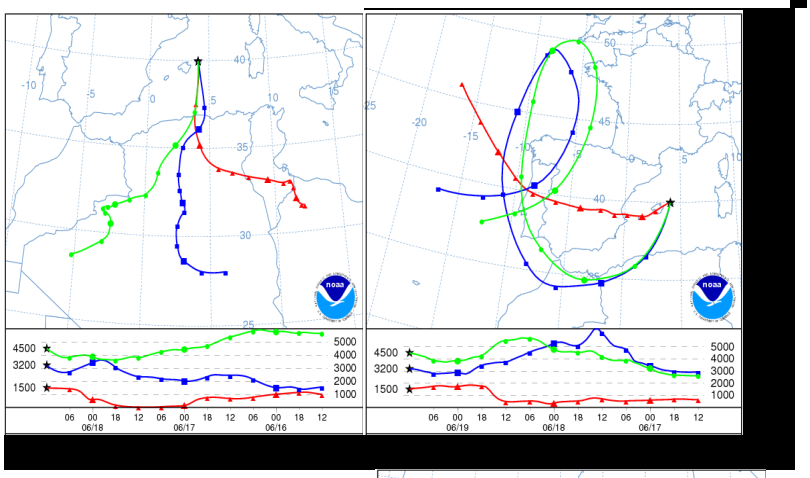

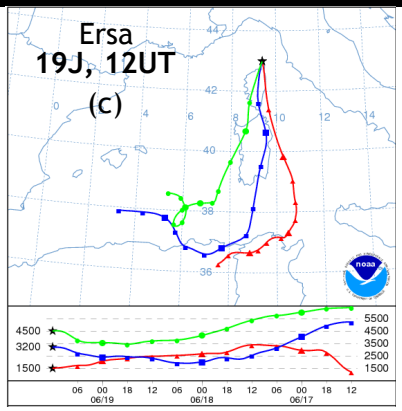

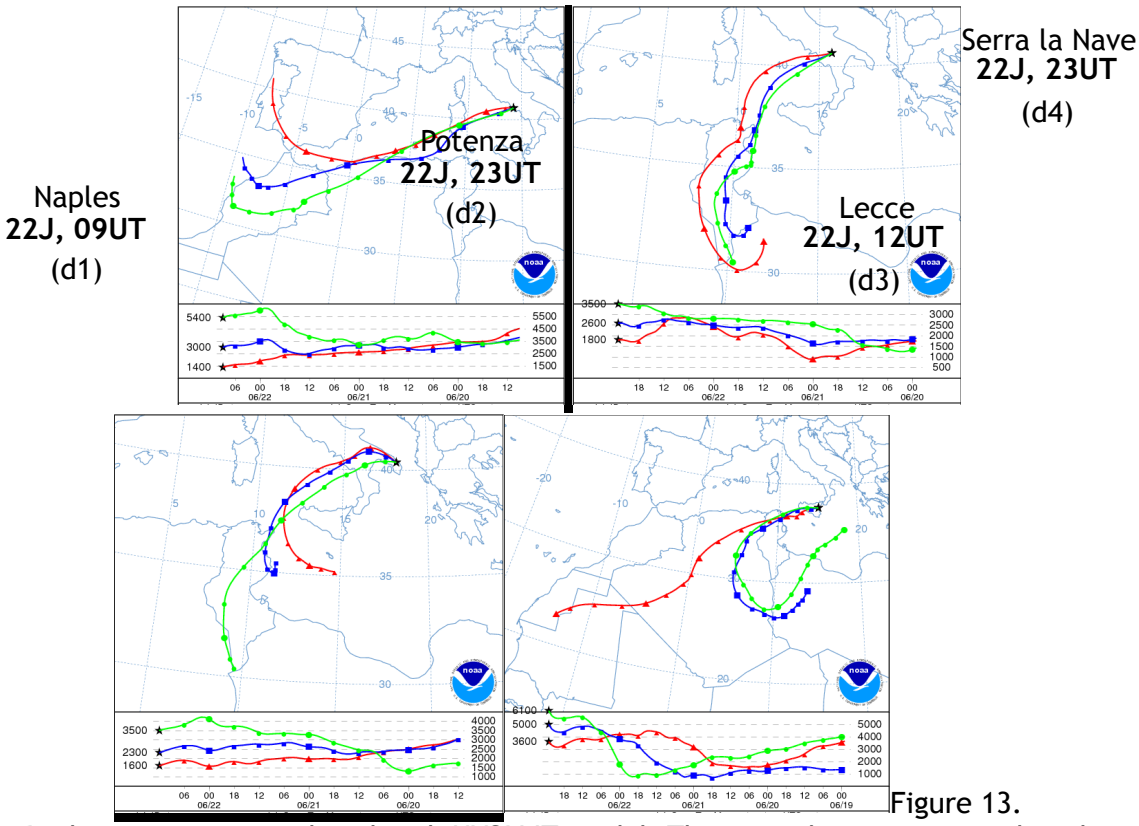

Figure 13. Backtrajectories simulated with HYSPLIT model. The green lines correspond to the top height of the dust layer, the red lines with the bottom height and the blue lines with the middle of the dust layer in each station calculated by the lidar measurements. 13a) are the back-trajectories for the Spanish peninsular stations. 13b) are the back-trajectories for Cap d'en Font. 13c) correspond to the back-trajectories in Ersa, and 13d) are the back-trajectories simulated for the Italian stations.

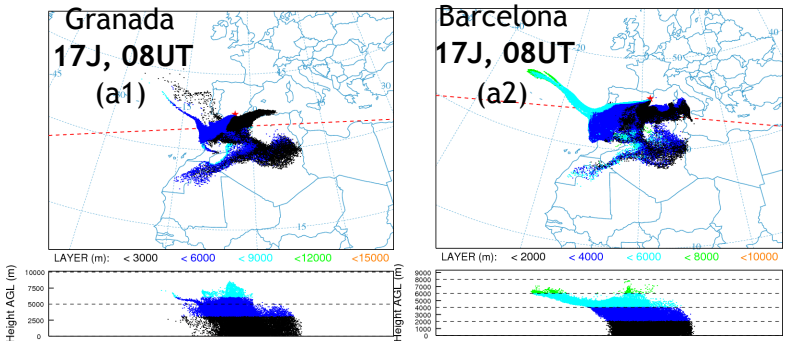

Cap d'en
16J, 08UT
(b1)

Cap d'en
17J, 08UT
(b2)

Cap d'en
18J, 08UT
(b3)

Cap d'en
19J, 08UT
(b4)

Ersa
19J, 12UT
(c)

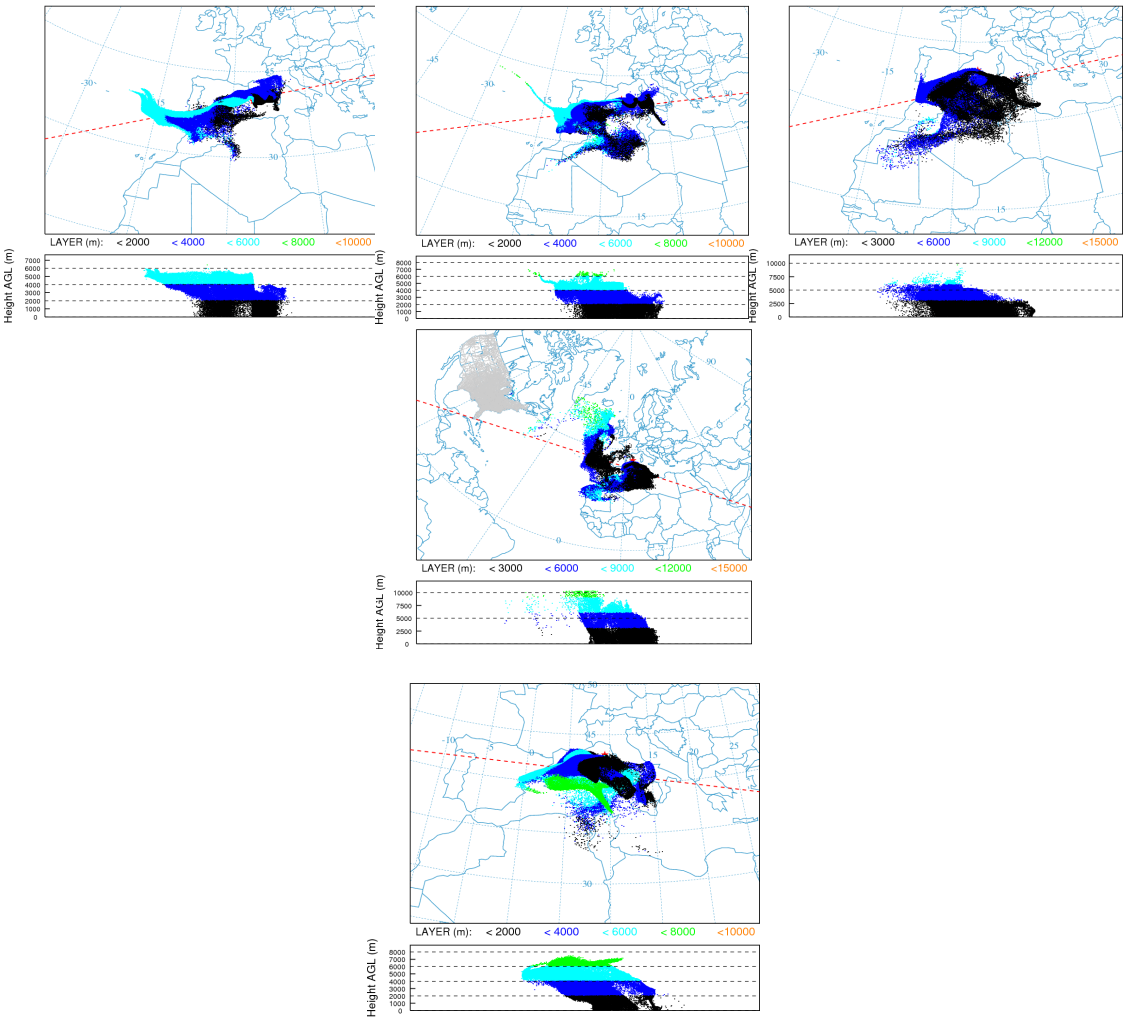

Naples
22J, 09UT
(d1)

Potenza
22J, 23UT
(d2)

Lecce
22J, 12UT
(d3)

Serra la Nave
22J, 23UT
(d4)

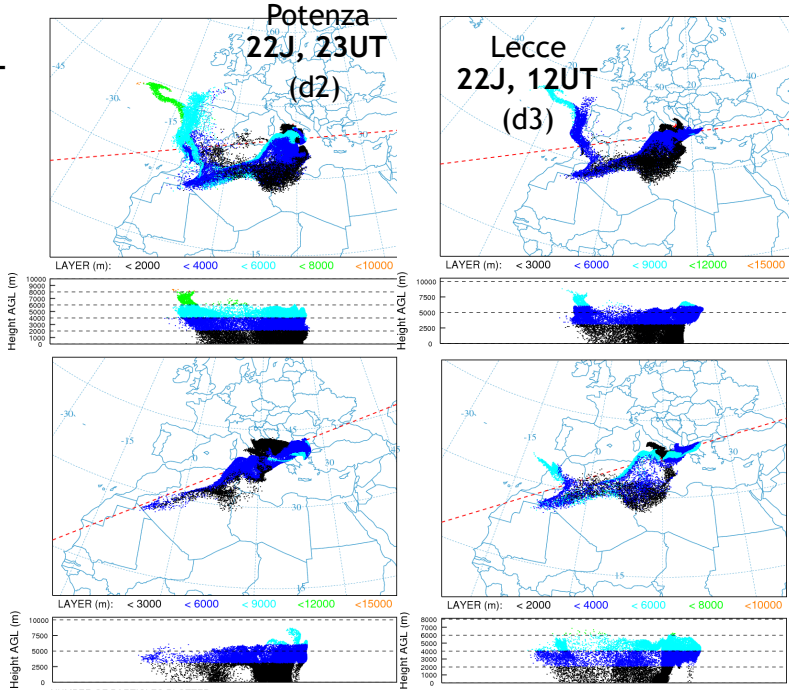

Figure 14. Particle positions simulated during 72 hours with HYSPLIT model. The green areas correspond to the top dust layers, the black areas with the bottom dust layers and the blue (clear and dark) areas with the middle dust layers in each station. 14a) are the particle positions for the Spanish peninsular stations. 14b) are

the particle positions for Cap d'en Font. 14c) correspond to the particle positions in Ersa, and 14d) are the particle positions simulated for the Italian stations. In the plots located in the lower part, the X axis indicates time and the Y axis indicates height AGL (m).